CREEP BEHAVIOR OF ULTRASONICALLY PROCESSED AZ91-NANO Al_2O_3 COMPOSITE

A DISSERTATION

Submitted in partial fulfillment of the

requirements for the award of the degree

of

MASTER OF TECHNOLOGY

In

METALLURGICAL AND MATERIALS ENGINEERING

(With specialization in Industrial Metallurgy)

By

NIKITA GOEL

DEPARTMENT OF METALLURGICAL AND MATERIALS ENGINEERING

INDIAN INSTITUTE OF TECHNOLOGY, ROORKEE

ROORKEE – 247667 (INDIA)

MAY-2016

CANDIDATE'S DECLARATION

I hereby declare that the work which is being presented in this dissertation entitled **"Creep Behavior of Ultrasonically Processed AZ91-Nano Al_2O_3 Composite"** in partial fulfillment of the requirements for the award of the degree of **Master of Technology** in **Metallurgical and Materials Engineering** with specialization in **Industrial Metallurgy**, submitted in the **Department of Metallurgy and Materials Engineering, Indian Institute of Technology Roorkee** is an authentic record of my own work carried out during the period from July 2015 to May 2016 under the supervision of **Dr. G. P. Chaudhari,** Associate Professor, Department of Metallurgical and Materials Engineering, Indian Institute of Technology Roorkee, India.

The matter presented in this dissertation has not been submitted by me for the award of any other degree.

Dated:
Place: Roorkee

Signature of the Candidate

(NIKITA GOEL)

CERTIFICATE

This is to certify that the above statement made by the candidate is correct to the best of my knowledge and belief.

Signature of Supervisor

(Dr G.P. Chaudhari)

Date:

Associate Professor

Metallurgical and Materials Engineering Department

Indian Institute of Technology Roorkee

ACKNOWLEDGMENT

This project is an outcome of many individuals. I am highly indebted to **Dr. G.P. Chaudhari**, Associate Professor, Department of Metallurgical and Materials Engineering, Indian Institute of Technology Roorkee, for encouraging me to undertake this dissertation as well as providing me all the necessary guidance and inspirational support throughout this dissertation work. It is my proud privilege to have carried out this dissertation work under his able guidance.

I wish to express my sincere thanks to **Dr. Anjal Sil**, Professor and Head of the Department, Metallurgical and Materials Engineering Department, Indian Institute of Technology Roorkee, for his help to carry out this dissertation.

I also like to express my gratitude to Mr. Neeraj Srivastava, Research Scholar for his innumerable discussion and his generosity and willingness to share his knowledge. I sincerely appreciate his valuable guidance and persistent encouragement in making this work.

Special thanks to technical staff of Metallography lab, Fabrication lab, Material Testing lab and others for their valuable supports, guidance and co-operations to carry out this dissertation. Thanks to MHRD, Govt. of India without whose generous funding and support, the project would have not been possible.

I would like to acknowledge all friends for their valuable information share, and developing love and confidence in me throughout the work. Last but not the least I would like to thank my parents for making my presence on this earth after which everything else was possible.

CONTENTS

	Page No.
1. Introduction	1
2. Literature Review	3
2.1 Strengthening Mechanism in nano composites	5
2.1.1 Strengthening by Grain Size Reduction	5
2.1.2 Orowan Strengthening Mechanism	5
2.1.3 Thermal Mismatch Strengthening	6
2.2 Ultrasonic Processing	7
2.3 Creep Mechanism	9
2.3.1 Creep mechanism in crystalline materials	13
2.3.2 Deformation mechanism of magnesium	17
3. Motivation and Objectives	20
4. Methodology	21
5. Experimental Methodology	22
5.1 Experimental	22
5.1.1 Materials and experimental set up	22
5.1.2 Experimental procedure	23
5.2 Microstructure Characterization	25
5.2.1 Sample preparation	25
5.2.2 Quantitative metallography	25
5.3 Mechanical Testing	27
5.3.1 Hardness testing	27
5.3.2 Tensile testing	28

5.3.3 Indentation or impression creep testing 29

6. Results and Discussions 32

6.1 Microstructural analysis 32

6.1.1 XRD Analysis 32

6.1.2 Optical Analysis 32

6.1.3 SEM Analysis 34

6.1.4 XRD results for nano composites 36

6.2 Mechanical Properties 37

6.2.1 Hardness results 37

6.2.2 Tensile results 37

6.2.3 Indentation creep results 39

7. Conclusions 51

8. Scope for future work 52

9. References 53

LIST OF FIGURES

FIG NO.	TITLE	PAGE NO.
2.1	Phase diagram of Mg-Al binary alloy	3
2.2	Orowan strengthening mechanism	6
2.3	Stages of distribution of nano particles by ultrasonic processing technique	8
2.4	Stages of creep failure	9
2.5	Relation between activation energy of self-diffusion and creep	11
2.6	Climb of an edge dislocation over an obstacle	14
2.7	Grain boundary sliding	15
2.8	Deformation mechanism map	16
2.9	Major planes in Hexagonal closed packed metals (Magnesium)	17
2.10	Deformation mechanism map of magnesium	18
5.1	Casting set up	23
5.2	Obtained casting of as-cast AZ91 alloy	24
5.3	LEICA Optical Microscope	26
5.4	Scanning Electron Microscope set up	26
5.5	X-ray diffraction setup	27
5.6	Vickers hardness testing machine setup	28
5.7	UTM machine for tensile testing	29
5.8	Sectioned samples for creep testing	30
5.9	Indentation creep testing machine set up	31
6.1	XRD pattern for nano Al_2O_3	32
6.2	Optical images of (a) as cast AZ91 alloy, (b) AZ91/0.5 wt% Al_2O_3 (c) AZ91/1 wt% Al_2O_3 and (d) AZ91/3 wt% Al_2O_3 nano composites.	33
6.3	SEM micrographs of (a) AZ91/0.5 wt% Al_2O_3, (b) AZ91/1 wt% Al_2O_3, (c) AZ91/3 wt% Al_2O_3 nano composites	35
6.4	XRD patterns ofAZ91 base alloy and fabricated nano-composites	36

6.5	Vickers hardness of the as-cast alloy and processed nano-composites	37
6.6	Stress strain curve of AZ91 and other nano composites	38
6.7	Creep curves for as cast AZ91 tested at (a) 448 K, (b) 473 K and (c) 498 K	40
6.8	Creep curves for AZ91/0.5 wt% alumina composites tested at (a) 448 K, (b) 473 K and (c) 498 K	41
6.9	Creep curves for AZ91/1 wt% alumina composites tested at (a) 448 K, (b) 473 K and (c) 498 K	42
6.10	Creep curves for AZ91/3 wt% alumina composites tested at (a) 448 K, (b) 473 K and (c) 498 K	43
6.11	ln $\dot{\varepsilon}$ versus ln σ plot for (a) AZ91/0 wt% alumina, (b) AZ91/0.5 wt% alumina, (c) AZ91/1 wt% alumina, (d) AZ91/3 wt% alumina	46
6.12	Plot of ln ε versus ln d at 448 K. The number in parenthesis is the average grain size of respective composite	48
6.13	Plot between ln $\dot{\varepsilon}$ and 1/T (K) for (a) AZ91/0 wt% alumina, (b) AZ91/0.5 wt% alumina, (c) AZ91/1 wt% alumina, (d) AZ91/3 wt% alumina at 222 MPa, 305 MPa and 388 MPa	49

LIST OF TABLES

TABLE NO.	TITLE	PAGE NO.
2.1	Values of creep exponent for different creep mechanisms	10
6.1	Grain size variation with increase in reinforcement wt%	34
6.2	Average size of nano particles and inter-particle distance for various processed nano compsoites	34
6.3	Tensile properties of different fabricated nano composites	38
6.4	Stress exponent values for various processed nano composites	47
6.5	Estimated increase in yield stress due to Orowan mechanism	50

ABSTRACT

The goal of this study is to evaluate core principles and to establish quantitative basis for the effects of ultrasonic processed AZ91-nano Al_2O_3 composite on the microstructure and creep properties. The nano composite was fabricated by adding 0%, 0.5%, 1% and 3% by weight Al_2O_3 (50 nm) to AZ91 alloy assisted by ultrasonic vibration. The ultrasonic vibrations distribute the nano particles uniformly in the melt, increases homogeneity and reduce segregation. The microstructures and mechanical properties of the produced composite are characterized Indentation creep tests are performed on the as cast and prepared nano composites at three different temperatures of 448 K, 473 K and 498 K and three different stresses of 222 MPa, 305 MPa and 388 MPa. Nano alumina additions increase the creep resistance of AZ91 alloy matrix with AZ91/3% alumina exhibiting the highest resistance. The creep behavior and dominant creep mechanism is studied further.

1. INTRODUCTION

The lightest structural metal currently in use is magnesium. It has wide applicability due to its high strength to weight ratio. By volume magnesium is 75% lighter than steel and 33% lighter than aluminum. Despite the lower density, magnesium alloys have comparable strength to weight ratio. They are preferred materials when looking for weight reduction without compromising overall strength. They are slowly replacing aluminum alloys for aerospace, electronics as well as automobile industries because of their lower density, excellent cast ability and workability, electromagnetic shielding capacity as well as higher damping capacity [1]. However their low strength, toughness and corrosion resistance limits their wide applications**.**

Magnesium alloys often employ aluminum, zinc, manganese, silicon, copper, rare earths alloying elements. Alloy AZ91 (Mg–9Al–0.8Zn–0.2Mn) is the most commonly used magnesium alloy. It has the widest application in magnesium cast products. It has better corrosion resistance, good dimensional stability, extremely good castability and superior mechanical properties as compared to other magnesium alloys. However, tendency for oxidation, low strength and poor creep resistance property at elevated temperatures limit its wide application [2]. In the AZ91 alloy matrix, low melting $Mg_{17}Al_{12}$ phase is present which softens at high temperature and thus shows poor creep resistance.

To improve the mechanical and creep resistance properties of AZ91 alloy, a more useful and effective method is dispersion hardening. It is an economical method to overcome the drawbacks of Mg alloys. Fabricating magnesium alloy MMCs with SiC, Al_2O_3, CNTs, TiO_2, etc. ceramic particles of micron size is widely used method to strengthen the matrix [3]. But it lowers the ductility, which limits their vast employment in industries. A more efficient and useful method is fabricating MMCs with nano-sized ceramic particles. They improve the strength without compromising on ductility [4]. Dislocation movement is hindered by these nano particles. They act as obstacles to the movement of dislocations and thus increase strength. This mechanism was first proposed by Orowan and thus commonly called as Orowan strengthening mechanism [5]. Also these nano ceramic particles exhibit excellent combination of high specific stiffness, high temperature mechanical properties and oxidation resistance. Therefore MMCs reinforced with nano particles can improve the high temperature properties of magnesium alloy matrix i.e. AZ91.

To fabricate metal matrix composites reinforced with ceramic particles of micron size, mechanical stirring is one of the most economical and most commonly used methods. But clustering in the melt occurs during fabrication of MMCs reinforced with nano particles. It is because they have much higher surface energy. Inducing ultrasonic vibrations in the melt is one of the most simple and effectively used physical methods to break the clusters and distribute nano particles uniformly in the melt. It reduces the segregation, increases homogeneity and changes the microstructure which includes grain refinement. It disperses and distributes nano scale particles uniformly in the melt [6]. Thus, high intensity ultrasound becomes a promising physical refining means to improve solidification structure. Various mechanisms have been proposed for the microstructural evolution under ultrasonic vibrations.

2. LITERATURE REVIEW

For this investigation, the material of interest is a commercial magnesium-aluminum based AZ91 alloy. The chemical composition of AZ91 alloy is listed as: [1]

Elements	Mg	Al	Zinc	Mn	Si	Cu	Ni	Fe
Contents (mass %)	Balance	9.30	0.71	0.21	0.10	0.03	0.005	0.002

Figure 2.1 show the phase diagram of Mg-Al binary alloy. The equilibrium liquidus and solidus temperatures of the AZ91 alloy are 598ºC and 468ºC. Its microstructure comprises of primary α-Mg and secondary β-$Mg_{17}Al_{12}$ phases.

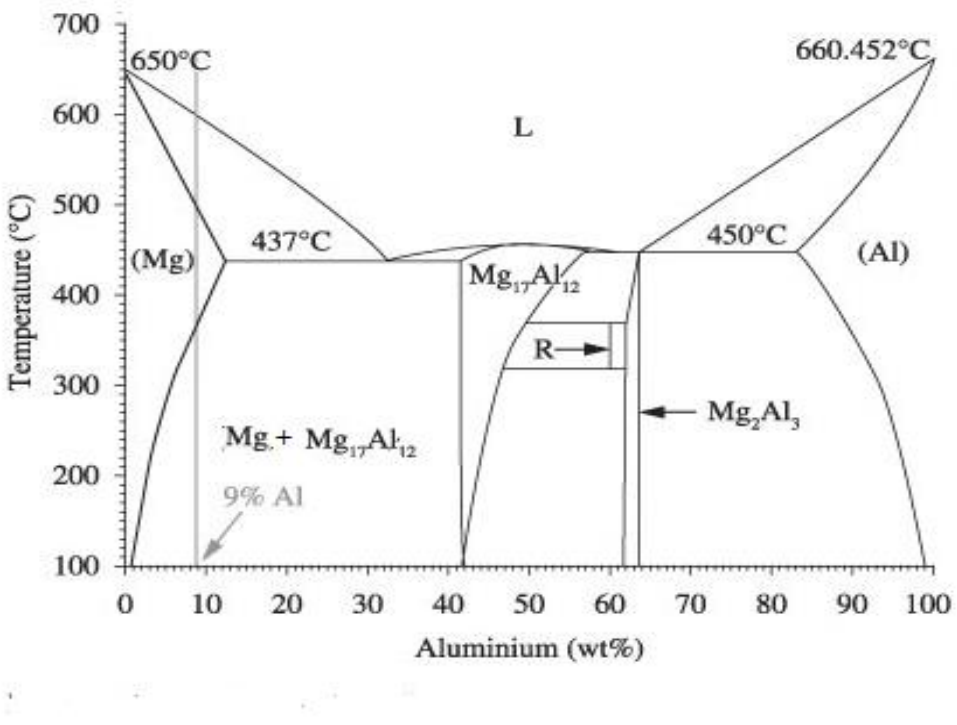

Fig.2.1- Phase diagram of Mg-Al binary alloy

Aluminum oxide is preferred choice for insulation, cutting and strengthening of materials etc. Chemically written as Al_2O_3, it is also called alumina. It has outstanding wear resistance property and exhibits good thermal stability. Also it is environment friendly and chemically inert towards bases and acids [7]. Nano sized alumina is more advantageous as compared to micron sized. It exhibits excellent combination of high specific stiffness, high temperature mechanical properties and oxidation resistance.

Alumina exists in different metastable phases such as gamma (γ) alumina, alpha (α) alumina, delta (δ). The crystal structure is different for different phases. Gamma-alumina structure is cubic, corundum or alpha alumina is hexagonal whereas delta is tetragonal. Gamma-alumina has low melting temperature, high activity and relatively small size. The main application includes production of synthetic sapphire. Alpha (α) alumina has good dimensional and phase stability and high hardness. It has wide range of applications which includes thermal fatigue resistance, as reinforcement in metal matrix composites etc.

K. Purazrang [3] worked on magnesium alloy reinforced with micron sized ceramic particles. Squeeze casting technique was employed for fabricating the metal matrix composite. 3μm sized δ short alumina fibers, were employed as reinforcement in AZ91 matrix. The alumina fibers were reinforced up to 20% by volume. With increase in the reinforcement content, fracture toughness and ductility got lowered.

M. Paramsothy [8] studied the AZ31/AZ91 hybrid alloy nano composites reinforced with nano alumina. Solidification process followed by hot extrusion was used to fabricate the composite. Compressive and tensile strengths of fabricated nano composite were improved as compared to the base alloy. Tensile failure strain of hybrid composite was enhanced due to the presence of uniformly distributed nano alumina.

2.1 Strengthening Mechanisms in Nano Composites

Material deformation depends upon ease of movement of dislocations. Strengthening occurs by impeding the motion of dislocations. Grain size reduction, Orowan strengthening mechanism and thermal mismatch strengthening are among the various methods of strengthening nano composites.

2.1.1 Strengthening by Grain Size Reduction

The finer the grains, the larger the area of grain boundaries that impedes dislocation motion. Toughness is also improved by grain size reduction. Hall-Petch equation 2.1 gives the effect of grain boundary strengthening.

$$\sigma_y = \sigma_o + \frac{k_y}{\sqrt{d}} \qquad (2.1)$$

Where σ_y is the yield stress, σ_o is a material constant, k_y is the strengthening coefficient, and *d* is the average grain diameter. According to this equation yield stress is inversely related to grain diameter. Hence, enhanced nucleation during solidification, by nano size particles, can be useful in improving the overall strength of the material.

2.1.2 Orowan Strengthening Mechanism

In Orowan mechanism the straight dislocation line approaches two particles. Dislocation bow out between two impenetrable particles and bends till it reaches its critical curvature and finally leaves dislocation loop around each particle. The formation of loops makes the dislocation movement more difficult, thereby increasing the strength of material. Figure 2.2 shows the mechanism of strengthening by Orowan. Mathematically it can be expressed by [5]

$$\tau_{\mathrm{Oro}} = \frac{0.13\mathrm{Gb}}{\mathrm{L}} \ln \frac{\mathrm{r}}{\mathrm{b}} \qquad (2.2)$$

Where *'b'* is the Burgers vector, *'G'* is the shear modulus of matrix and *'r'* and *'L'* denotes particle size and inter particle distance between dispersions respectively. Coarse micron sized particles have large inter-particle spacing. Hence strengthening by Orowan mechanism is not significant. However strength is increased by reinforcing alloy matrix by nano alumina particles (50 nm). Ultrasonic treatment disperses the nano particles uniformly in the melt and thus

decreases the inter-particle spacing. Equation 2.3 gives the mathematical expression for calculating L:

$$L = \frac{4r(1-f)}{3f} \qquad (2.3)$$

Where 'f' is the precipitate volume fraction.

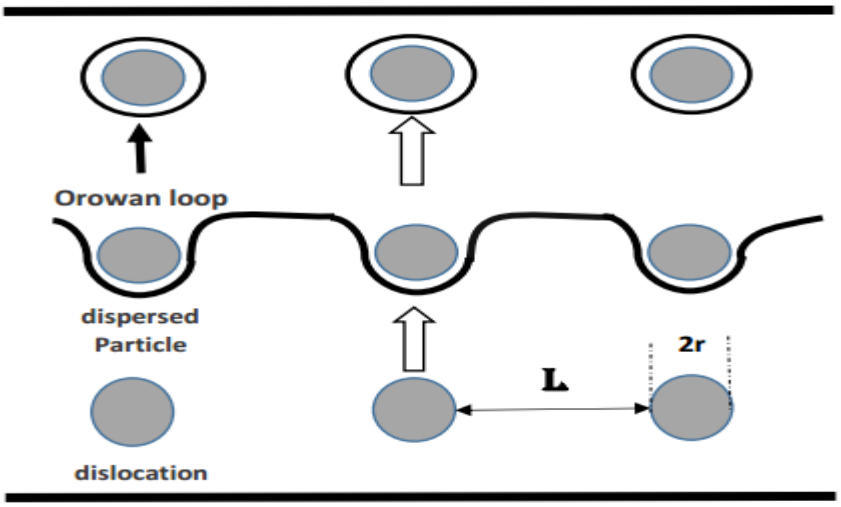

Fig.2.2- Orowan strengthening mechanism

2.1.3 Thermal Mismatch Strengthening

Nano alumina particles and Mg alloy matrix have different CTE. Because of the thermal mismatch between the reinforcement and the matrix, great amount of dislocation density is generated during cooling of composite. Equation 2.4 gives the mathematical expression for calculating $\Delta\sigma_{CTE}$ [5]

$$\Delta\sigma_{CTE} = \eta G b\sqrt{\rho} \qquad (2.4)$$

Where *'ρ'* is the dislocation density and *'η'* is the constant.

2.2 Ultrasonic Processing

The various methods for uniform dispersion of reinforced particles in molten material include [9]:

1. Mechanical stirring

2. Ultrasonic vibration

3. Electromagnetic vibration techniques

To fabricate micro particles reinforced metal matrix composites, methods like squeeze casting, powder metallurgy and mechanical stirring have been commonly used. But clustering and agglomeration occurs in the melt during fabrication of MMCs reinforced with nano particles. It is because they have much higher surface energy and low wettability. During ultrasonic processing treatment (UST), vibrations of high frequency are induced in the melt. Ultrasonic processing not only distributes the nano particles into the molten metal, but promotes dendritic fragmentation which leads to grain refinement.

The various effects of ultrasonic vibrations on the properties of as cast materials are [10]

1. Uniformity in the distribution of non-metallic inclusions

2. Improvement of homogeneity in the melt

3. Reduction in dendritic segregation and formation of equiaxial grain

4. Refinement in mean grain size

Figure 2.3 shows clearly shows the underlying mechanism for the ultrasonic treatment of the melt. The cavities formed due to pressure variation fig (a) are imploded and shock waves are generated fig (b) leading to broken fragments, which distribute inside the melt fig (c).

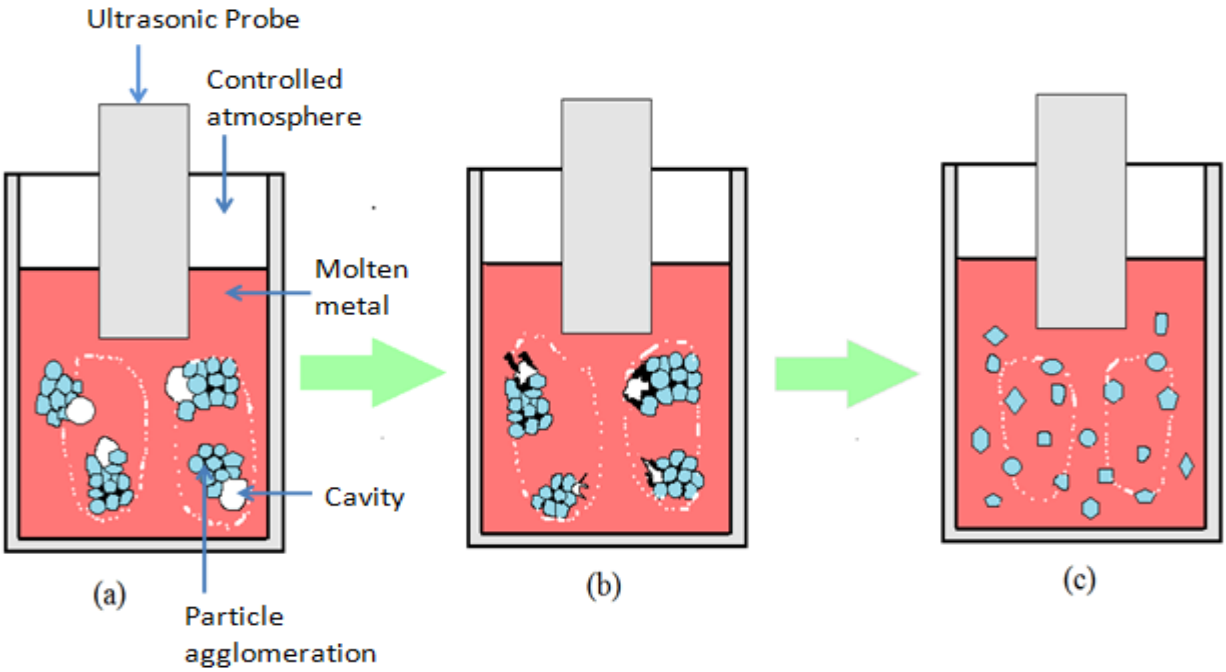

Fig.2.3-Stages of distribution of nano particles by ultrasonic processing technique.

Lan et al. [1] worked on AZ91D alloy reinforced with nano silicon carbide particles. They used ultrasonic treatment to distribute the particles uniformly in the molten matrix. Dispersion of silicon carbide nano particles was greatly enhanced by using the ultrasonic treatment. Although some clustering was still there, but it was very less in comparison to composites fabricated by conventional stirring process. They suggested that during ultrasonic treatments the cavities which are formed due to pressure variations are imploded and shock waves are generated which leads to broken fragments to distribute inside the molten metal. They also concluded that with the increase in the amount of silicon carbide nano particles, micro hardness of composite also got increased.

G. Cao [4] studied the mechanical properties of AZ91D/1.0 wt% AlN nano particles of average size 25 nm synthesized using the ultrasonic treatment. The yield and tensile strength of the nano composite was significantly improved with the retention of ductility.

2.3 Creep Mechanism

Time dependent, slow and progressive deformation in a material, which is under a constant stress and constant high temperature, is known as creep. A plot of strain (ε) vs. time (t) represents the creep deformation. Figure 2.4 shows the creep deformation.

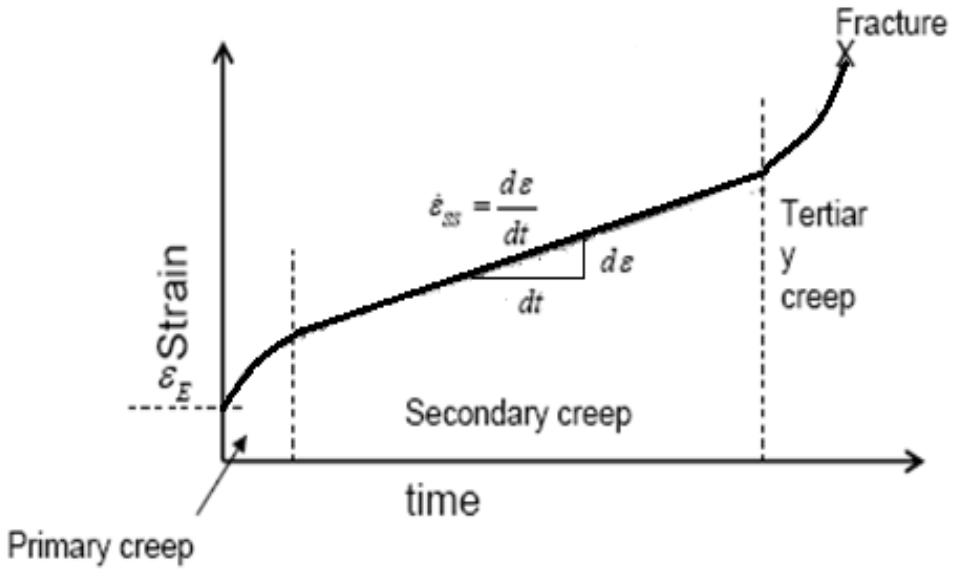

Fig.2.4-Stages of creep failure

Tensile creep curve shows three regions or stages. The first stage of the creep known as primary creep or transient creep, in which creep rate decreases with time. In primary creep, material gets strain hardened because of which creep resistance of the material increases. It is the dominant process at low temperature and stress. The second stage or region of the creep curve is known as secondary creep or viscous creep. In this stage the creep rate is nearly constant. Due to this constant creep rate this region is also called as steady state creep. The third region in creep curve is known as tertiary region or stage. This stage occurs due to the change in dimensions of the material which results in an increase in stress and due to which creep rate increases up to fracture. Tertiary region is not observed in compressive creep. It is due to the constant stress in compression creep but in tensile, due to change in dimensions of the specimen stress is not constant.

Equation 2.5 gives the mathematical expression for steady state creep [11]

$$\dot{\varepsilon} = \frac{A\sigma^n}{d^q T}\exp\left(-\frac{Q}{RT}\right) \quad (2.5)$$

Where *'n'* and *'q'* are the stress exponent and grain size exponent, respectively. *Q* is the activation energy for creep, *T* is the absolute temperature and d is the average grain diameter. Activation energy is the measure of the energy barrier that must be overcome for molecular motion to occur. In this equation, steady state creep rate ($\dot{\varepsilon}$) is affected by stress σ, average grain diameter d, and absolute temperature T. The values of coefficient A, Q, exponents 'n' and 'q' depends upon material and dominating creep mechanism that is acting. The values of stress exponent 'n' and grain size exponent 'q' for different creep mechanisms are outlined in table 2.1.

Table 2.1- Values of creep exponent for different creep mechanisms [11]

Name of mechanism	**'n'**	**'q'**	**Description**
Diffusional flow (*Nabarro-Herring Creep)*	1	2	Vacancy diffusion through the crystal lattice.
Diffusional flow (*Coble Creep)*	1	3	Vacancy diffusion along the grain boundaries.
Grain boundary sliding	2	2 or 3	Sliding accommodated by vacancy diffusion through the crystal lattice (q=2) or along grain boundaries (q=3)
Dislocation creep (*Power law Creep)*	3 to 8	0	Dislocation motion, with climb over the microstructural obstacles.

Equation 2.6 is the Arrhenius-type equation for steady state creep rate [12].

$$\dot{\varepsilon} = Ae^{-Q/RT} \qquad (2.6)$$

Where,

Q = activation energy

A = constant factor

T = temperature (K)

R = universal gas constant

The values of activation energy are determined by plotting the graph between ln ε̇ and ln (1/T) for a constant stress and the slope of the line gives the –Q/R values. The magnitude of the activation energy gives the nature of active mechanism controlling the creep process.

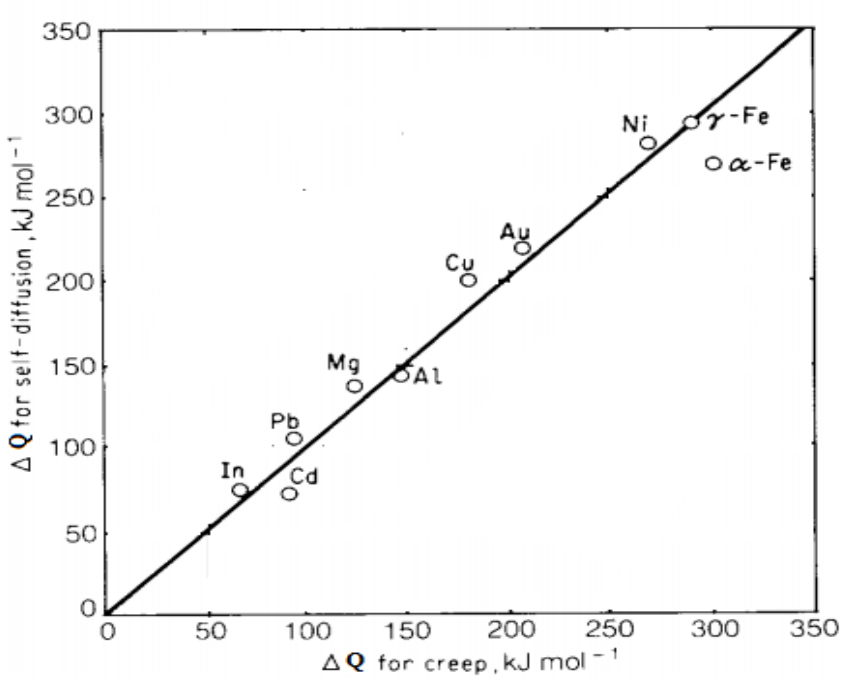

Fig.2.5- Relation between activation energy of self-diffusion and creep [12].

Figure 2.5 shows the extensive correlation between the activation energy of high temperature creep and activation energy for self-diffusion for pure metals. The activation energy in case of self-diffusion is strongly related to the formation and movement of vacancies, which supports to the view that dislocation climb aided by vacancy diffusion is the rate controlling creep at high temperature.

The stress exponent as per Norton equation is shown in equation 2.8 [12]

$$\dot{\varepsilon} = A\sigma^{n}\exp^{(-\frac{Q}{RT})} \quad (2.8)$$

Or $$\ln \dot{\varepsilon} = \ln A + n\ln\sigma - Q/RT \quad (2.9)$$

The values of stress exponent *'n'* are determined by plotting the graph between ln $\dot{\varepsilon}$ and ln σ at a constant temperature and the slope of the line gives the values of 'n'. The obtained values of stress exponent 'n' describes the dominant creep mechanism taking place in the material as given in table 2.1. Generally the values of stress exponent lie in between 3 to 8 for most of the metals, value of 5 being the most common.

2.3.1 Creep mechanism in crystalline materials

Creep deformation in crystalline materials comprises of three different mechanisms such as [11, 12]

1. Diffusional creep
2. Dislocation creep
3. Grain boundary sliding

Operating mechanisms depend on the nature of material, applied stress and homologous temperature.

Diffusional creep

This mechanism involves the movement of vacancies in the crystal lattice. This mechanism occurs at low stress but requires relatively high temperatures. Vacancies are created at or near the grain boundaries. And this results in concentration gradient (of vacancies) due to which vacancies move or diffuse to regions of lower concentration. This movement or diffusion of vacancies is favored by high temperature. If the diffusion of vacancies occurs through the lattice, the mechanism is known as Nabarro- Herring creep. Nabarro-Herring creep is described by the equation 2.10 [12]

$$\dot{\varepsilon} = \frac{14\sigma b^3 D_v}{kTd^2} \qquad (2.10)$$

Where D_v is lattice diffusion coefficient and 'd' is the average grain diameter. This equation makes clear that the creep rate is directly proportional to stress 'σ' (n = 1) and inversely proportional to the square of the average grain diameter (q=2).

If the vacancies diffuse or move through the grain boundaries, then it is called as Coble creep and described by equation 2.11 [12]

$$\dot{\varepsilon} = \frac{50\sigma b^4 D_{gb}}{kTd^3} \qquad (2.11)$$

Where D_{gb} is grain boundary diffusion coefficient. In this equation also the creep rate is directly proportional to stress but inversely proportional to the cube of the average grain diameter 'd'

(q=3). This shows that both types of diffusional flow i.e. Nabarro-Herring creep and Coble creep are essentially a viscous process.

Dislocation creep

It involves movement of dislocations by climb over the barrier. It is also referred as power law creep. This mechanism occurs by dislocation glide aided by diffusion of interstitials and vacancies. Figure 2.6 show that due to stress application the edge dislocation moves along a slip plane and during movement, it encounters an obstacle (precipitation particle or other immobile dislocations). So to continue its movement the edge dislocation climbs over the obstacle by diffusion of atoms.

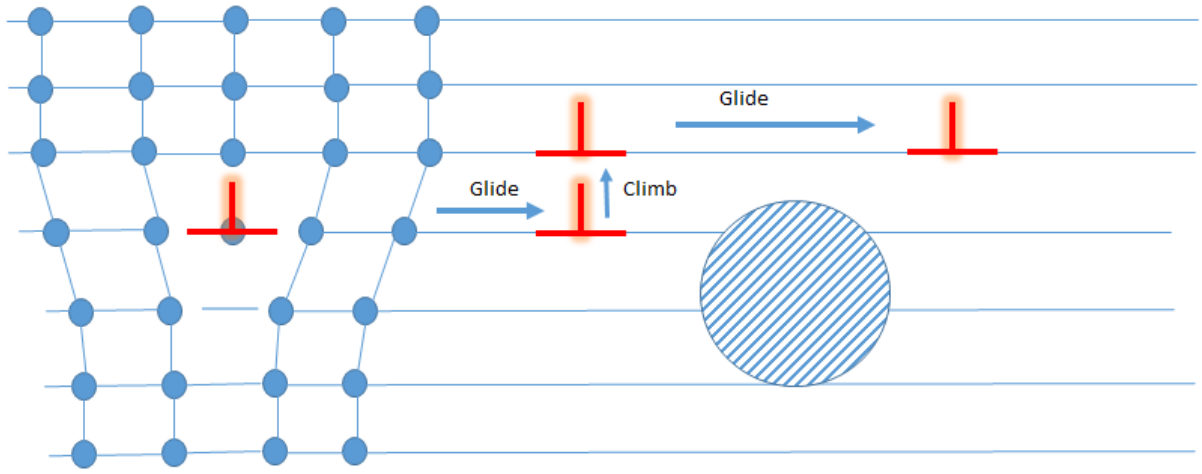

Fig.2.6-Climb of an edge dislocation over an obstacle

Creep experiments with a range of metals shows that the stress exponent 'n' varies from 3 to 8. The power law relation expressed in equation 2.12 [12], describes the steady state creep

$$\dot{\varepsilon} = \frac{AGbD_v}{kT}(\sigma/G)^n \qquad (2.12)$$

Where $\dot{\varepsilon}$ is the steady creep rate, A is material's constant, G is the shear modulus, D_v is the coefficient of diffusion, b is the Burgers vector, k is the Boltzmann constant, T is temperature (K) and 'n' is the stress exponent.

Diffusion coefficient is expressed as given in equation 2.13

$$D_{v=}\ D_0 \exp(-\frac{Q}{kT}) \qquad (2.13)$$

Where Q is the activation energy. By combining equations 2.12 and 2.13, we get

$$\dot{\varepsilon} = \frac{AGbD_0}{kT}(\sigma/G)^n \exp(-\frac{Q}{kT}) \qquad (2.14)$$

The dislocation creep mechanism is independent of grain size. The value of the grain size exponent is zero (q=0).

Grain boundary sliding

This mechanism involves sliding of grains past each other. It is an important creep mechanism occurring in polycrystalline materials deformed at high temperatures. Figure 2.7 shows the sliding of grains past each other.

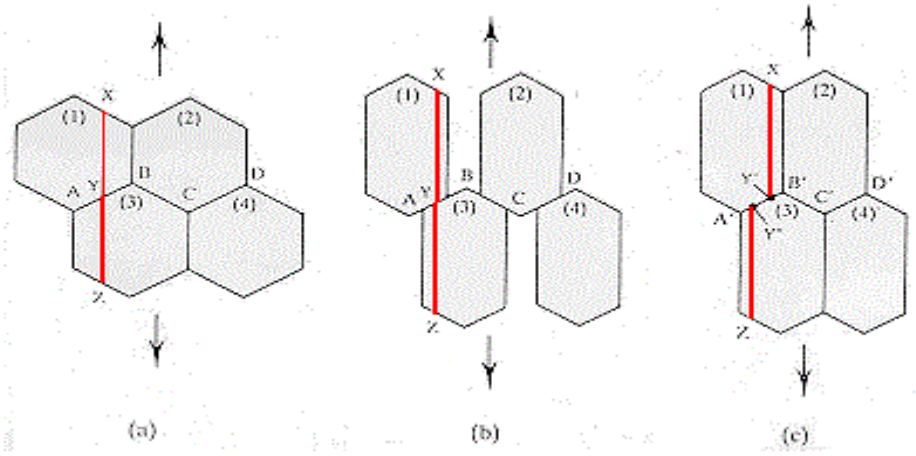

Fig.2.7- Grain boundary sliding [11]

Figure 2.7 (a) shows polycrystalline material prior to creep. In figure (b) voids are formed at the grain boundary during diffusion assisted flow. Figure (c) shows the grain boundary sliding occurring to keep material from falling apart. Grain boundary sliding mechanism occurs in materials with a small grain size. Grain boundaries have a large number of broken bonds and at high temperature, the movement of vacancies and atoms at grain boundaries is more and this

results in weakening of grain boundaries. Due to stress application these weak grain boundaries slide over each other and the material deforms easily.

Deformation mechanism maps developed by Ashby and co-workers [12] are the best practical way of illustrating and utilizing the consecutive equations for the various creep deformation mechanisms. These maps are plotted in between normalized stress and homologous temperature as shown in figure 2.8. The various regions of the map show the dominating creep mechanism at a particular stress and temperature.

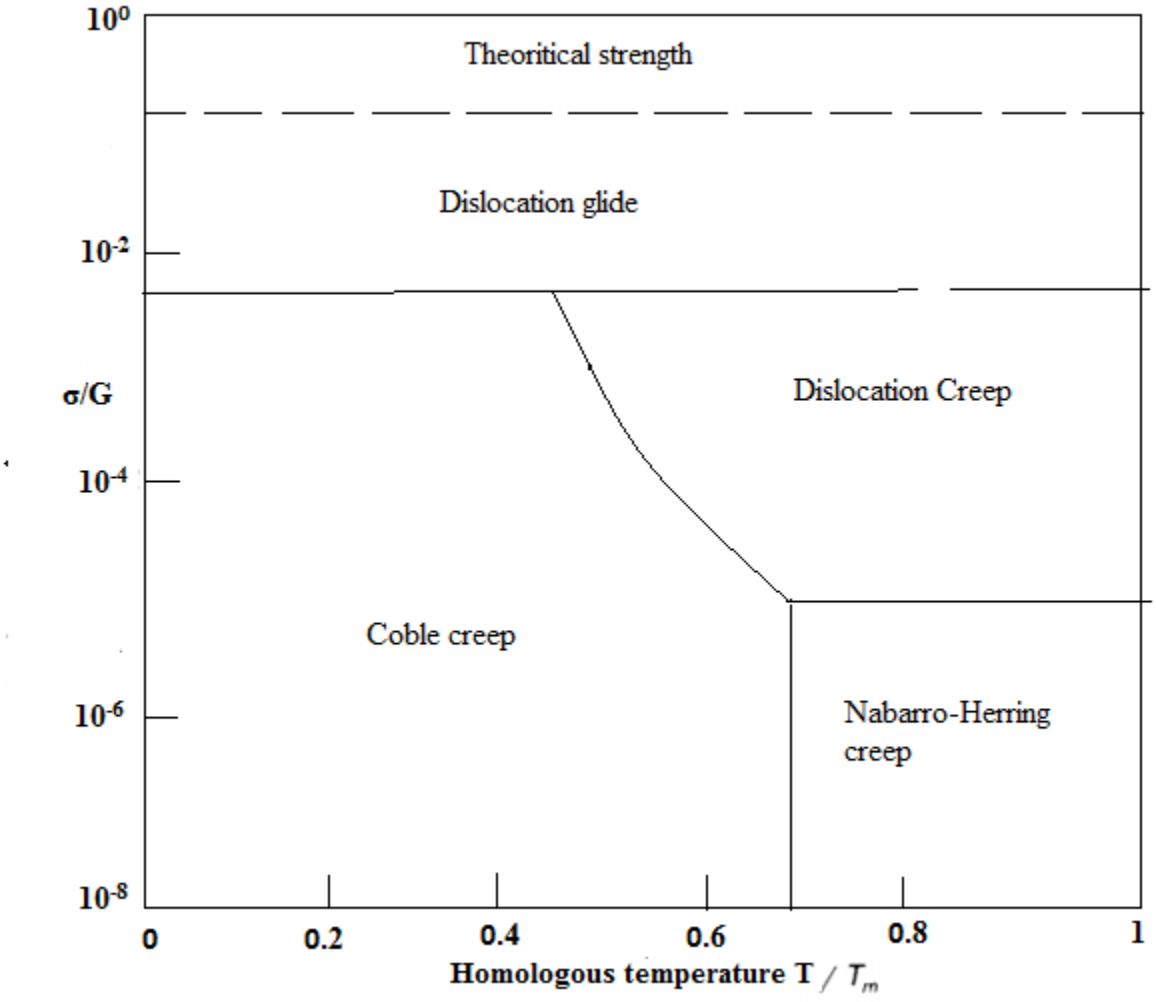

Fig.2.8-Deformation mechanism map [12]

2.3.2 Deformation mechanism of magnesium

As the crystal structure of magnesium is hexagonal closed packed, it has a limited number of slip systems at room temperature. Deformation of magnesium at room temperature occurs by slip and twinning. At low or room temperature slip occurs only on basal plane [13]. Major planes of magnesium crystallite (hcp) are shown in figure 2.9.

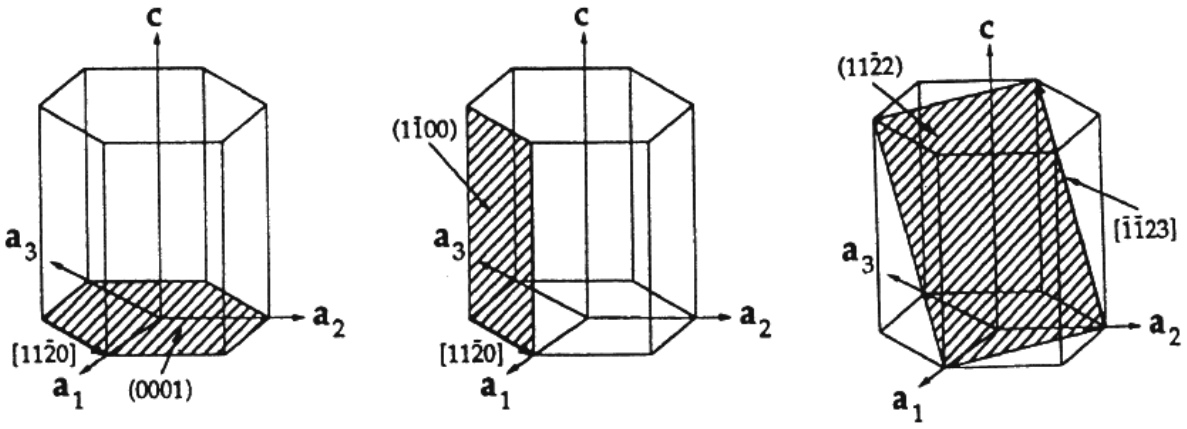

Fig.2.9-Major planes in Hexagonal closed packed metals (Magnesium) [13]

.

Literature survey suggests that at low temperature creep deformation is mostly due to twinning and slip on basal planes. Although at high temperature the other non-basal planes such as prismatic and pyramidal planes gets activated and play an important role in creep deformation. At high temperature diffusion of atoms through the grain boundaries is more, due to which grain boundaries get weakened and this results in grain boundary sliding by a small application of load.

The dominating creep mechanism in magnesium depends upon stress and homologous temperature as shown in figure 2.10 [14]. At high temperature and low stresses the dominating creep mechanism is diffusional flow whereas at moderate temperature and high stresses dislocation creep is the controlling creep mechanism.

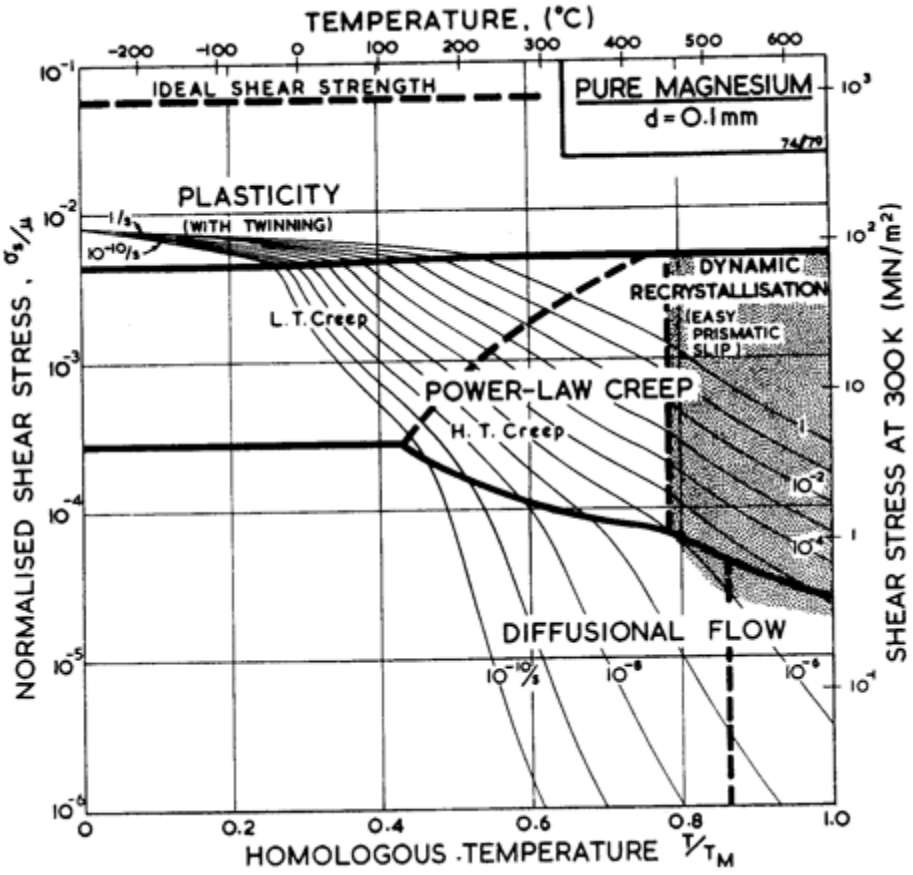

Fig.2.10- Deformation mechanism map of magnesium [14]

A. Srinivasan [15] studied the effect of intermetallic phases on creep properties of AZ91 magnesium alloy. Silicon and antimony were intentionally added to AZ91 alloy to form thermally stable intermetallic phases into the matrix. Creep tests were carried out at 150°C and 200°C with an initial stress of 50 MPa on the as-cast samples. These intermetallic phases enhanced the creep resistance of the material due to superior thermal stability at high temperatures.

Harish Kumar [16] studied the effect of nano alumina additions on impression creep behavior of AS41 MMCs. Uniform dispersion of nano Al_2O_3 in the melt was obtained by mechanical stirring and ultrasonic processing. Impression creep tests were carried out in temperature range of 175°C-225°C with the applied stress ranging from 109.2 MPa to 140.4 MPa. Creep resistance of AS41 was significantly improved by introducing nano Al_2O_3 as reinforcement. They came to a conclusion that pipe diffusion was the main creep controlling mechanism.

Diao Yu-Shou [17] investigated the strengthening effect of nano alumina on 6061Al matrix. The composite with 5 vol% and 7 vol% Al_2O_3 (20-100 nm) fabricated ultrasonically shows homogeneity in the casting. Also by introduction of nano Al_2O_3 as reinforcement, creep resistance of 6061Al MMCs was greatly enhanced with 5 vol% Al_2O_3 composite exhibiting the highest resistance.

3. MOTIVATION AND OBJECTIVES

These days number of materials are discovered or produced to meet the demands of high temperature applications. However, with technological developments there is need for even better high temperature strength and other properties like light weight. Magnesium has the lowest density among all metals present in the world. They have vast application in aerospace, electronics, and automotive industries. Their advantages include high damping capacity, good castability, electromagnetic shielding capacity, low density etc. But due to poor creep resistance and low strength at high temperature, these are unsuitable for many of the components in automobile engines.

AZ91 alloy being used in 90% of all magnesium cast products is the most favored magnesium alloy. But low strength and poor creep resistance property at elevated temperatures limit its wide application [2]. Because metal matrix composites reinforced with hard, thermally stable nano particles can yield better creep resistance, it is useful to design such composites and investigate the impression or indentation creep of magnesium alloy AZ91 and its nano composite. The objectives of present investigation are therefore:

- To identify the effects of ultrasonic treatment on the distribution of nano alumina reinforcement.
- To study the effect of AZ91 nano alumina composite on the various mechanical properties like hardness and tensile strength.
- Introduction of nano Al_2O_3 particles in the AZ91 alloy to enhance its creep resistance and to investigate the dominant creep mechanisms in AZ91 alloy and their nano composites at different temperatures and different stresses.

4. METHODOLOGY

In the current research work, the nano composite is prepared by addition of nano alumina (50 nm) in the AZ91 matrix. The material is melted at 700°C temperature and castings are prepared by addition of 0.5%, 1%, 3% alumina in the matrix assisted by ultrasonic vibrations for about 3 minutes. One as cast sample was also prepared for the comparison of the properties.

Firstly the characterization of alumina powder is carried out by performing XRay Diffraction (XRD) of nano alumina to know its composition.

Then, Microstructural analysis of all the samples is done using optical microscope as well as Scanning Electron Microscope (SEM). This reveals the nano particle dispersion. Further to get a clear view about the phases present XRay Diffraction (XRD) is carried out.

Hardness measurements are carried out on a Vicker's hardness tester with 1Kg load for all the samples and the trend from as cast to 3% Al_2O_3 addition is observed and relation between Vicker's hardness number and the amount of Al_2O_3 is established.

Tensile studies are done on a Ultimate tensile testing machine to know the change in mechanical properties like yield strength, total elongation, stress to failure, ultimate tensile strength through which a conclusion will be drawn regarding the strength of the nano composite.

Finally, the aim of work is to study the effect of nano ceramic particles present in the Mg alloy matrix on the creep behavior. So indentation creep tests are carried out on the creep testing machine at different stresses and temperatures. Also stress exponents and activation energies are calculated to find the dominant creep mechanism.

5. EXPERIMENTAL METHODOLOGY

5.1 Experimental

5.1.1Materials and experimental set up

Commercial AZ91 magnesium alloy was taken as the base material. It has a nominal composition of 9 wt% aluminum, 1 wt% zinc and rest magnesium. Alumina particles which are used as reinforcement in this research have an average grain size of 50 nm. To fabricate magnesium alloy metal matrix composite reinforced with nano alumina, mechanical stirring accompanied by ultrasonic treatment was carried out. Mild steel crucible was used to melt the charge in an electric resistance furnace. Figure 5.1 shows the experimental set up.

Ultrasonic processing unit (Model VCX 1500 from Sonics and Materials, USA) comprises of an acoustic radiator made of Ti-6Al-4V alloy, an air cooled converter which is made of piezoelectric lead zirconate titanate crystal (PZT), a 20 kHz acoustic generator, a 1500 watt electric power supply, a probe and a booster. Time of processing is precisely controlled during the ultrasonic treatment of all the melts to get uniform effect of ultrasonic vibrations in the composites. Also, the vibration amplitude (60μm) which is used in ultrasonic processing is same for every casting.

Fig.5.1- Casting set up

5.1.2 *Experimental procedure*

Nano composites with 0.5 wt% alumina, 1 wt% alumina and 3 wt% alumina were fabricated. 250 grams of AZ91 was melted for every casting by heating it to 700°C. A thermocouple was positioned near the molten metal to determine the temperature throughout the experiment. Nano

alumina particles were preheated to a temperature of 400°C. When the alloy had been melted, these preheated particles were added to it. Then the melt was stirred mechanically for about 10-15 minutes. Soon thereafter, heating of melted charge (700°C) was done for 15-20 minutes. After that ultrasonic treatment of the melt was done by dipping preheated ultrasonic probe in it. It was carried out for 3 minutes.

Coating of zirconia was applied on the probe to avoid sticking of melt to it. Thereafter the molten material contained in the mild steel crucible was air cooled. Figure 5.2 shows the obtained casting of as cast AZ91 alloy. Similar casting was done to obtain as-cast AZ91 alloy samples for comparison.

Fig.5.2- Obtained casting of as-cast AZ91 alloy.

5.2 Microstructure characterization

Microstructural characterization of as cast AZ91alloy and their nano composites with 0.5 wt% alumina, 1 wt% alumina and 3 wt% alumina was carried out. Analysis included identification of chemical composition of different phases in the materials. Crystallography involved identifying crystal structure and determining different phases present in the material. Structural morphology involved identifying the shape, size and distribution of these phases.

5.2.1 Sample preparation

The samples for microstructural analysis were sectioned from the middle of the casting. Then these samples were prepared by paper polishing on silicon carbide emery paper up to 2000 grit size. After that they were cloth polished with fine cloth using powder MgO. After polishing, the samples were washed with methanol and electro-etched with solution of 60 ml H_3PO_4, 100 ml ethanol at 3V for 25 seconds.

5.2.2 Quantitative metallography

The microstructural analysis was done using optical microscope (Leica DMI 5000M microscope). Distribution of nano particles was investigated using LaB_6MA18 Zeiss scanning electron microscope (SEM). Figure 5.3 and 5.4 shows the optical microscope and scanning electron microscope, respectively. Grain size was calculated by linear intercept of 10 optical micrographs of each sample.

X-ray diffraction analysis was done on Bruker D8 machine using Cu-Kα radiation scanning in the range of 20-90°. The scan rate used was 2°/minute. White powder nano alumina as well as prepared composites were analyzed. Figure 5.5 shows the X-ray diffraction set up machine.

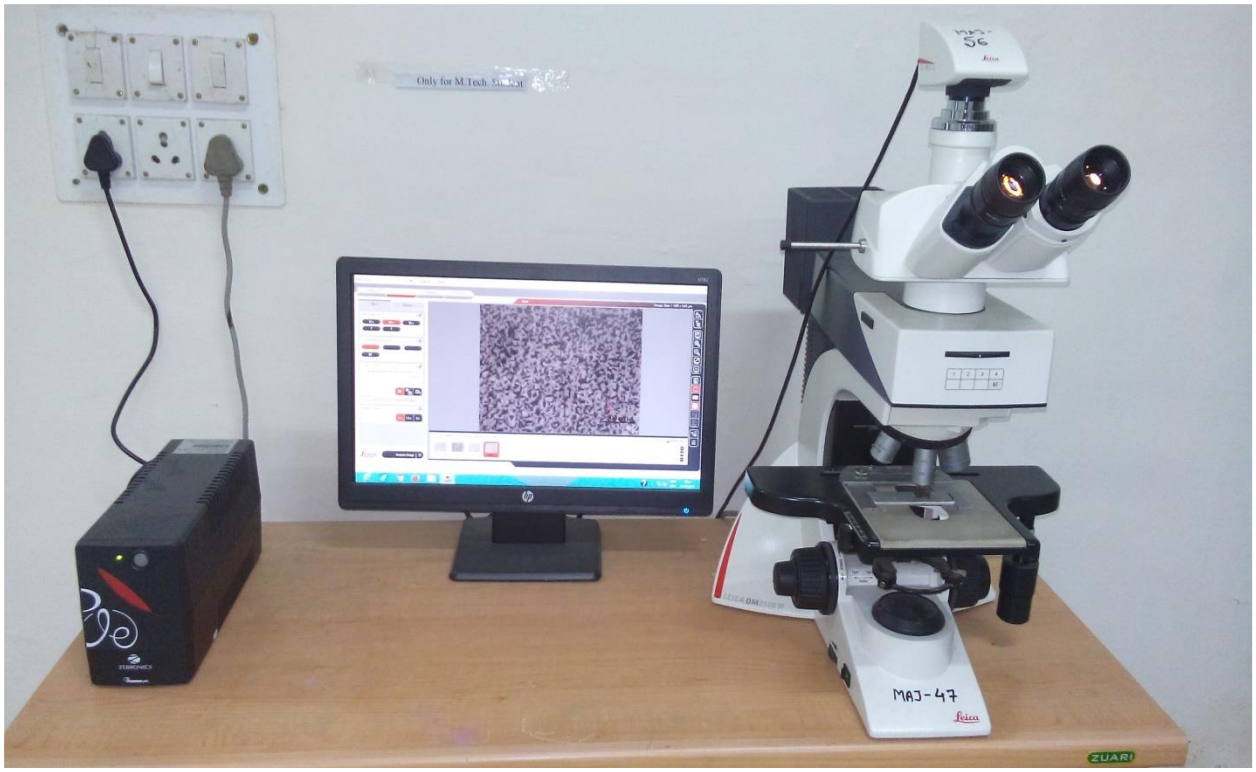

Fig.5.3- LEICA Optical Microscope

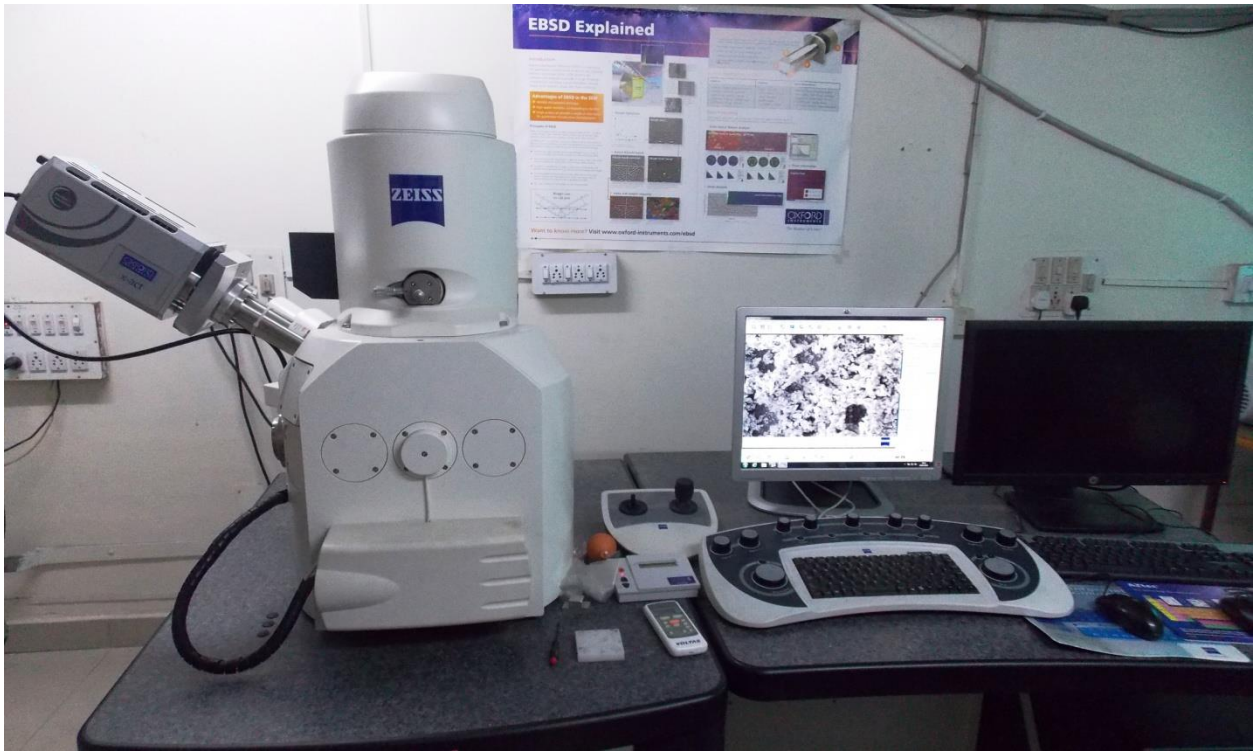

Fig.5.4- Scanning Electron Microscope set up

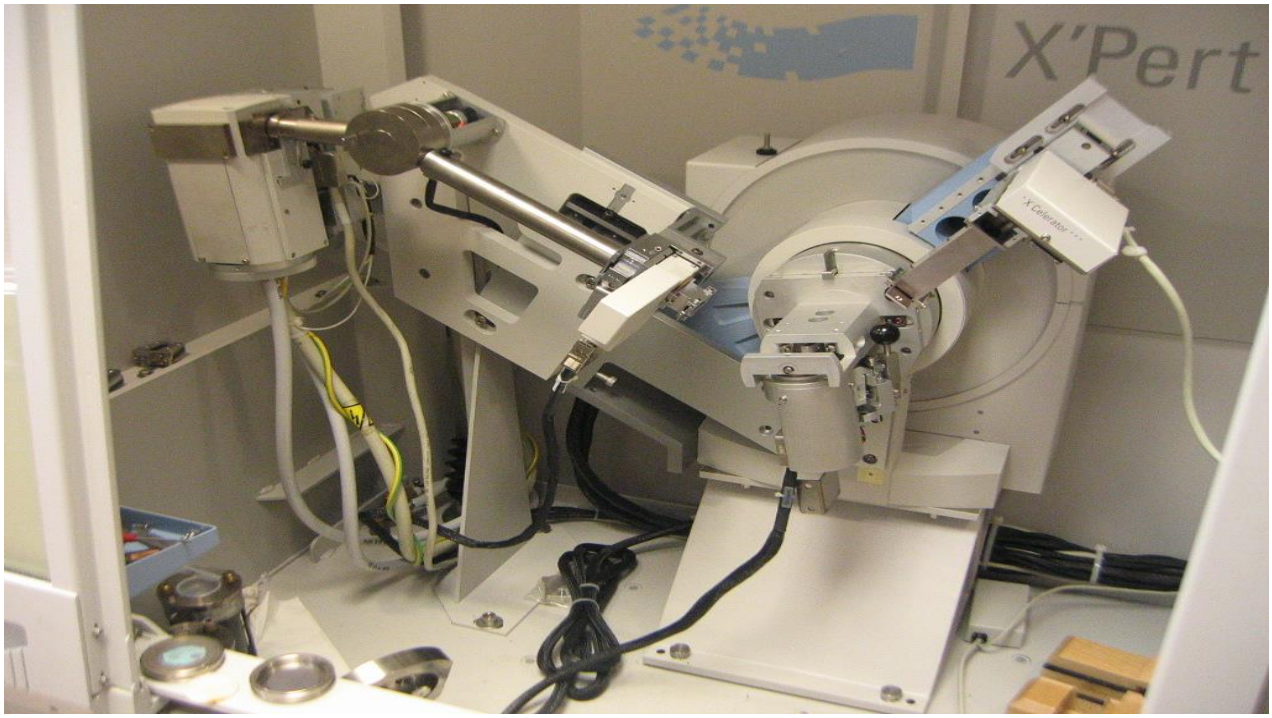

Fig.5.5- X-ray diffraction setup.

5.3 Mechanical testing

5.3.1 Hardness testing

Hardness was measured for the as-cast AZ91 alloy, AZ91/0.5 wt% Al_2O_3, AZ91/1 wt% $Al_2O_3$and AZ91/3 wt% Al_2O_3composites by Vickers hardness testing machine (FIE-VM50PC) with a load of 1 kg and dwell time of 10 seconds. For each sample test was repeated 5 times and then mean value was calculated. Samples were prepared by paper polishing on silicon carbide emery paper up to 1500 grit size. After that they were cloth polished with fine cloth using powder MgO for precise measurement of the indentation. Figure 5.6 shows the set up for hardness testing.

Fig.5.6- Vickers hardness testing machine setup

5.3.2 Tensile testing

The tensile properties were determined by conducting tensile test on Tinius Olsen Universal testing machine (Model PS-30) for as cast AZ91 and fabricated nano composites. For each composite, three tensile specimens were prepared for error free measurement. Figure 5.7 shows the UTM machine set up.

Fig. 5.7 UTM machine for tensile testing

5.3.3 Indentation or impression creep testing

Creep tests were carried out on the indentation or impression creep machine. For the creep experiments, samples of size 15 mm x 15 mm x 7 mm were sectioned from the middle of each casting with the use of power hacksaw. Sectioned samples for the creep testing are shown in

figure 5.8. Thereafter these cut samples were ground on SiC emery papers up to 1500 grit to get smooth finish for accurate and precise measurement of depth of indentation.

In a creep test, at specified load and temperature, tungsten carbide indenter of diameter 1.5 mm is impressed or pushed against the sample's surface. The curves showing depth of indentation as a function of time were obtained from where we can calculate the minimum creep rate. Here impression creep tests were done on as-cast AZ91 alloy, AZ91/0.5 wt% Al_2O_3, AZ91/1 wt% Al_2O_3 and AZ91/3 wt% Al_2O_3 composite samples at temperatures of 175°C, 200°C and 225°C and stresses of 222 MPa,305 MPa and 388 MPa for 10000 seconds. To prevent oxidation of creep samples the tests were done under a vacuum of 10^{-7} Pa.

Fig. 5.8- Sectioned samples for creep testing

For creep testing SPRANKTRONICS indentation creep machine of 100 kg capacity was utilized. Creep samples were placed in a vacuum chamber to minimize oxidation occurring at high temperature. Its various parts include rotary and diffusion pump vacuum system, water cooling arrangement, specimen chamber, LVDT, load and temperature indicator units, lever arm, data acquisition system and dedicated software, tubular furnace. The set up for indentation creep testing machine is shown in the figure 5.9.

Fig.5.9- Indentation creep testing machine set up

6. RESULTS AND DISCUSSION

6.1 Microstructural analysis

6.1.1 XRD Analysis

XRD pattern of nano powder Al_2O_3 (50 nm) is shown figure 6.1 which confirms that the constituted gamma (γ) alumina.

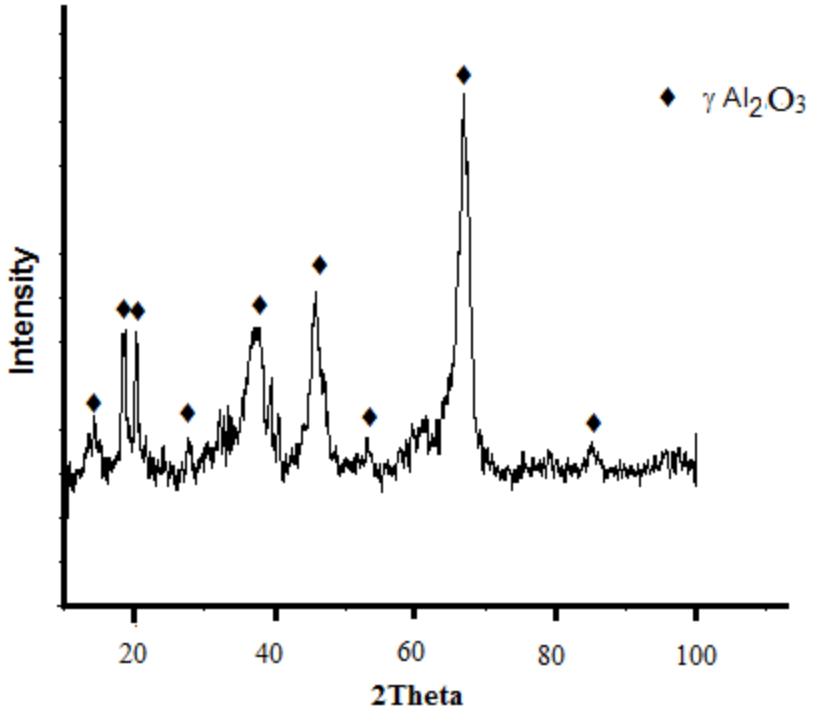

Fig.6.1- XRD pattern for nano Al_2O_3

6.1.2 Optical Analysis

Figure 6.2 (a), (b), (c) and (d) shows the optical images of as cast AZ91 alloy, AZ91/0.5 wt% Al_2O_3, AZ91/1 wt% Al_2O_3, and AZ91/3 wt% Al_2O_3 nano composites, respectively. The phases present include α-Mg matrix, β-$Mg_{17}Al_{12}$ and eutectic mixture. The poor creep property of AZ91 is because of this low melting β phase. At higher temperature it becomes soft and coarse. Also, the amount of eutectic mixture is less in the as cast AZ91 alloy. However, it significantly increased as the alumina content is increased.

Figure 6.2 (a) shows the relatively coarse dendritic structure. Figure 6.2 (b), (c) and (d) shows the replacement of this coarse dendritic structure by a finer structure. Relative grain size of AZ91 and its nano composites are summarized in table 6.1. Slight reduction in grain size can be attributed to reinforcing nano Al_2O_3 particles which act as active sites for nuclei formation. Such preferential sites favor the process of heterogeneous nucleation and thus refine the grain size. Although there is reduction in grain size by almost 23%, the refinement is not very significant due to the fact that ultrasonic processing was performed above the liquidus temperature, and the mechanism of dendrite fragmentation was not operative.

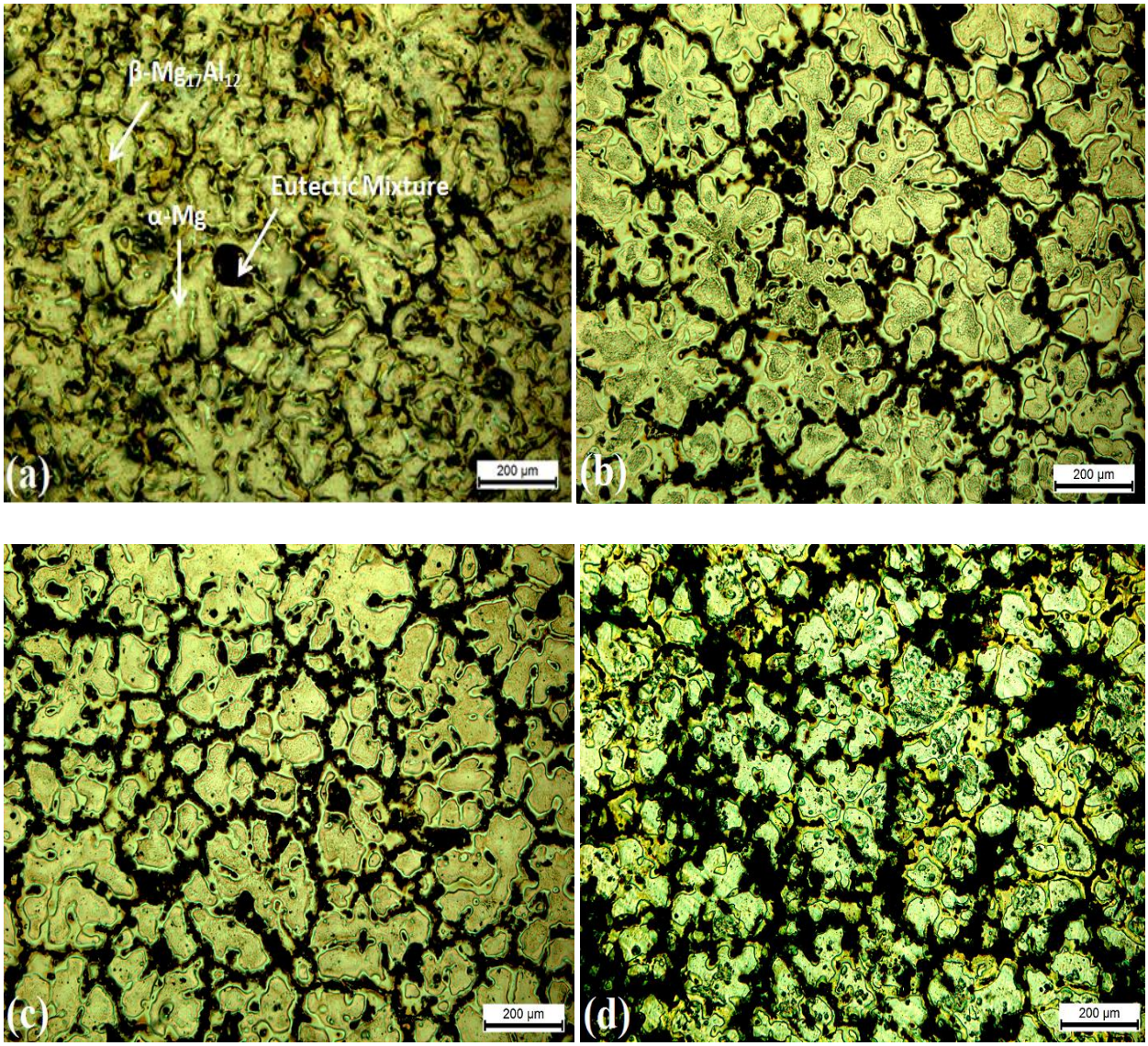

Fig.6.2- Optical images of (a) as cast AZ91 alloy, (b) AZ91/0.5wt% Al_2O_3 (c) AZ91/1wt% Al_2O_3 and (d) AZ91/3wt% Al_2O_3 nano composites.

Table 6.1 Grain size variation with increase in reinforcement wt%

Reinforcement wt%	0	0.5	1	3
Average grain size (μm)	245	217	202	187

6.1.3. SEM Analysis

Figure 6.3 shows the SEM images of (a) AZ91/0.5 wt% alumina, (b) AZ91/1 wt% alumina, (c) AZ91/3 wt% alumina composites. Figure (a) shows fewer particles with fewer agglomerates whereas figure (c) shows large number of nano particles as a result of increment in wt% of alumina. Uniform dispersion of nano Al_2O_3 particles with little agglomeration, in the α-Mg matrix is clearly visible. It is due to ultrasonic processing done during the fabrication of the composite. Figure 6.3 (b) and (c) shows the reduced inter particle spacing between nano alumina particles with increase in the alumina content. Thus there was 23% decrement in inter particle spacing for 1 wt% alumina and 65% for 3 wt% alumina as compared to 0.5 wt% alumina. Table 6.2 shows the various parameters deduced from figure 6.3.

Table 6.2- Average size of nano particles and inter-particle distance for various processed nano compsoites

Mg alloy composite	Average size of nano particles(nm)	Inter-particle distance(nm)
AZ91/0.5 wt% Al_2O_3	77	359
AZ91/1 wt% Al_2O_3	98	278
AZ91/3 wt% Al_2O_3	122	124

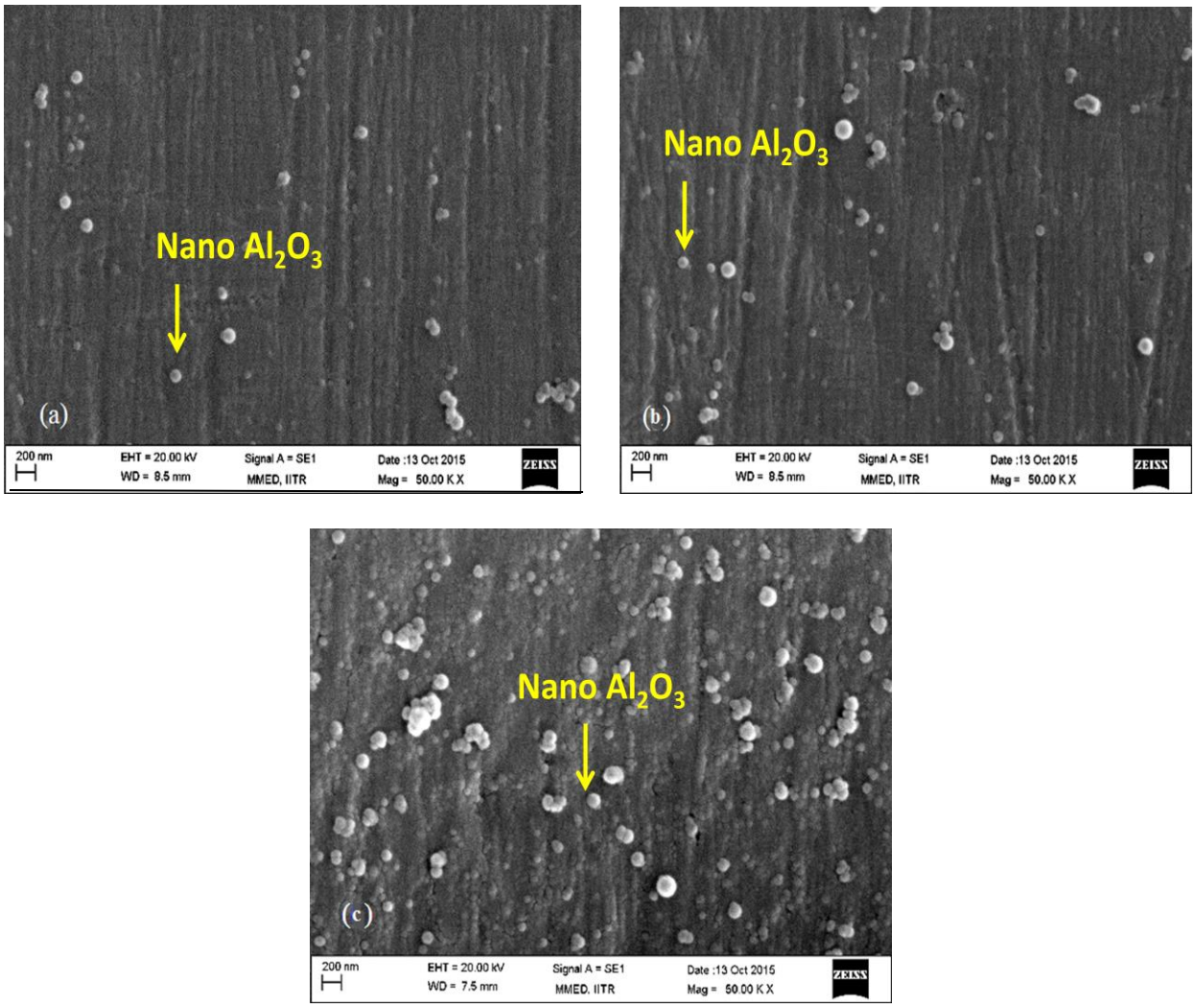

Fig.6.3-SEM micrographs of (a) AZ91/0.5 wt% Al_2O_3, (b) AZ91/1 wt% Al_2O_3, (c) AZ91/3 wt% Al_2O_3 nano composites

6.1.4 XRD results for nano composites

XRD patterns for nano composites are depicted in the figure 6.4. Pattern for the as cast AZ91 confirms the presence of α Mg, $Mg_{17}Al_{12}$. For the nano composites, in addition to these phases, alumina peaks were also visible.

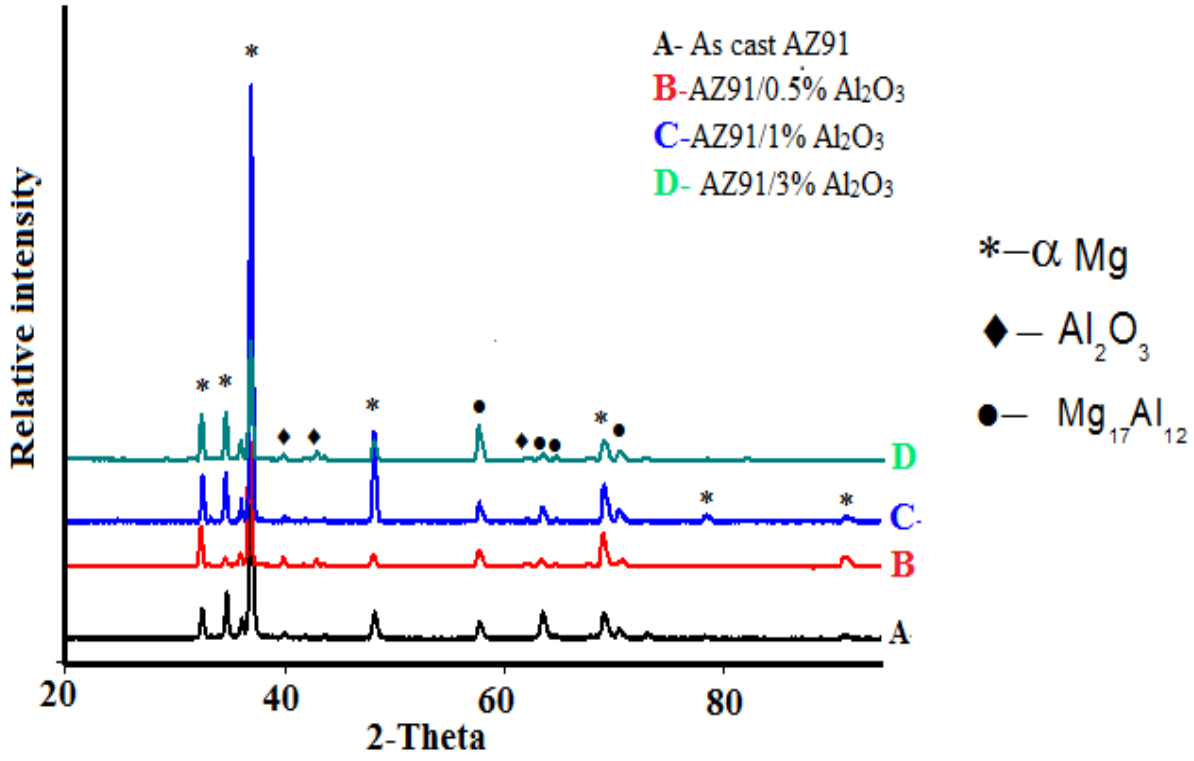

Fig. 6.4- XRD patterns ofAZ91 base alloy and fabricated nano-composites.

6.2 Mechanical properties

6.2.1 Hardness results

Figure 6.5 represents the hardness value for the processed nano composites as a function of increasing alumina content. Vickers hardness number for different fabricated nano composites is increased as compared to AZ91 alloy. Nano alumina which is present inside the matrix makes the movement of dislocations difficult, hence strengthening it and leading to the increase in hardness value.

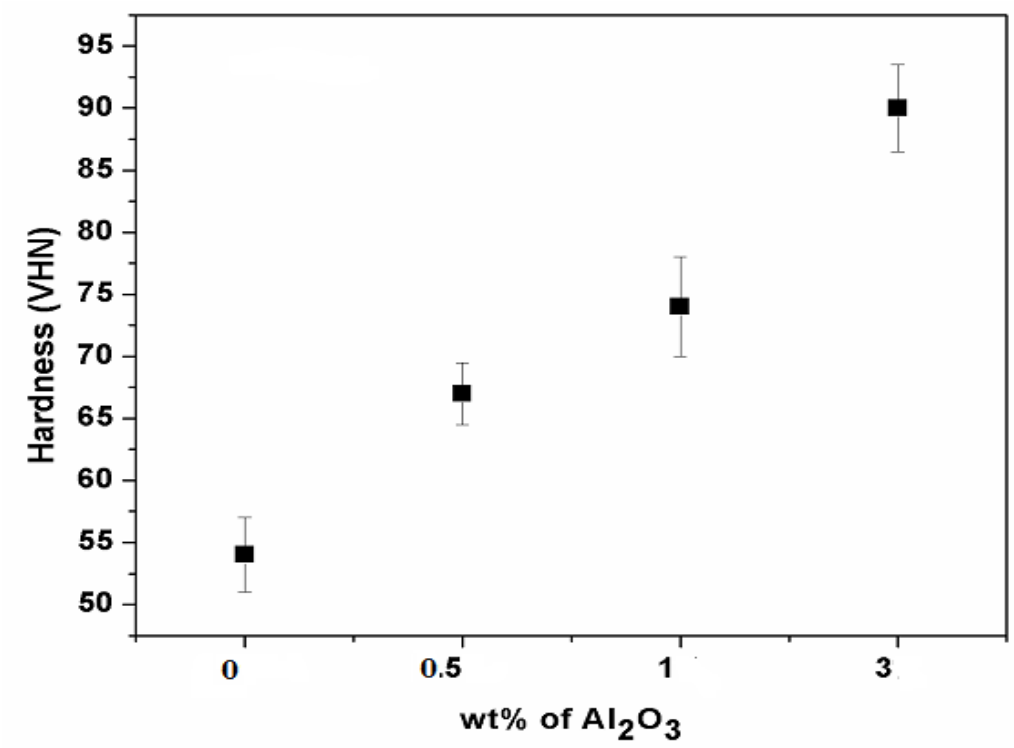

Fig.6.5- Vickers hardness of the as-cast alloy and processed nano-composites.

6.2.2 Tensile results

The tensile related tests were carried out on Universal testing machine (UTM) machine. Figure 6.6 depicts the variation of engineering strain with engineering stress. There is enhancement of tensile properties from as cast AZ91 to AZ91/ Al_2O_3 nano composite with AZ91/ 3 wt% Al_2O_3 showing the highest properties. Also there is an enhancement of ductility from about 2% of as

cast AZ91 to 3% of AZ91/ 3 wt% Al_2O_3. Table 6.3 shows the various properties of as cast AZ91 alloy and other nano composites.

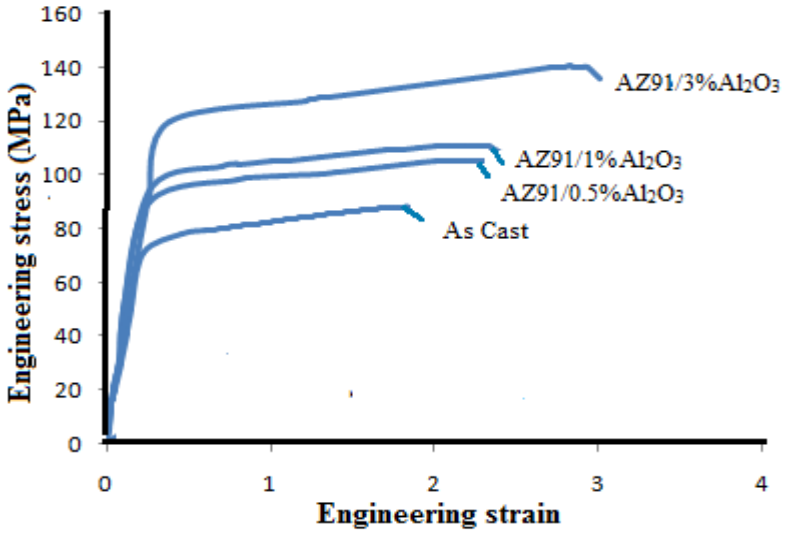

Fig. 6.6- Stress strain curve of AZ91 and other nano composites

Table 6.3- Tensile properties of different fabricated nano composites.

Material	Yield Strength	Ultimate tensile Strength	Elongation (%)
As-cast AZ91 alloy	75±3	88±3	1.96±0.22
AZ91/ 0.5wt%Al_2O_3	90±2	106±3	2.4±0.2
AZ91/ 1wt%Al_2O_3	97±3	110±2	2.44±0.31
AZ91/ 3wt%Al_2O_3	120±4	140±5	2.92±0.28

Slight enhancement in ductility for AZ91 nano alumina compositesis basically due to combined effects of [18]:

a) Grain refinement

b) Presence of uniformly dispersed reinforcement particles

c) Activation of non-basal slip system

Hexagonal closed packed metals are particularly benefitted from grain refinement in ductility enhancement as in these intergranular fracture arises from intercrystalline stresses. Also, dispersed phases in brittle matrix, which restricts the dislocation mobility and thus favors the crack generation, acts as ductility enhancer, a phenomena opposite to in ductile matrix. Dispersed reinforcement particles in brittle metal matrix (i) provides sites where cleavage cracks may open ahead of an advancing crack front, (ii) dissipate the stress concentration which would otherwise exist at the crack front, and (iii) alter the local effective state of stress from plane strain to one of plane stress in the neighborhood of the crack tip. Additionally, through recent studies it has been understood that non-basal slip system activates under axial tensile stress and thus increases ductility.

6.2.3 Indentation creep results

Figure 6.7, 6.8 and 6.9 and 6.10 shows the obtained impression creep curves for different AZ91 nano alumina composites. In these curves primary region followed by secondary region can be seen. Tertiary creep is not observed in these creep curves. It is due to the constant stress in compression creep but in tensile, due to change in dimensions of the specimen stress is not constant.

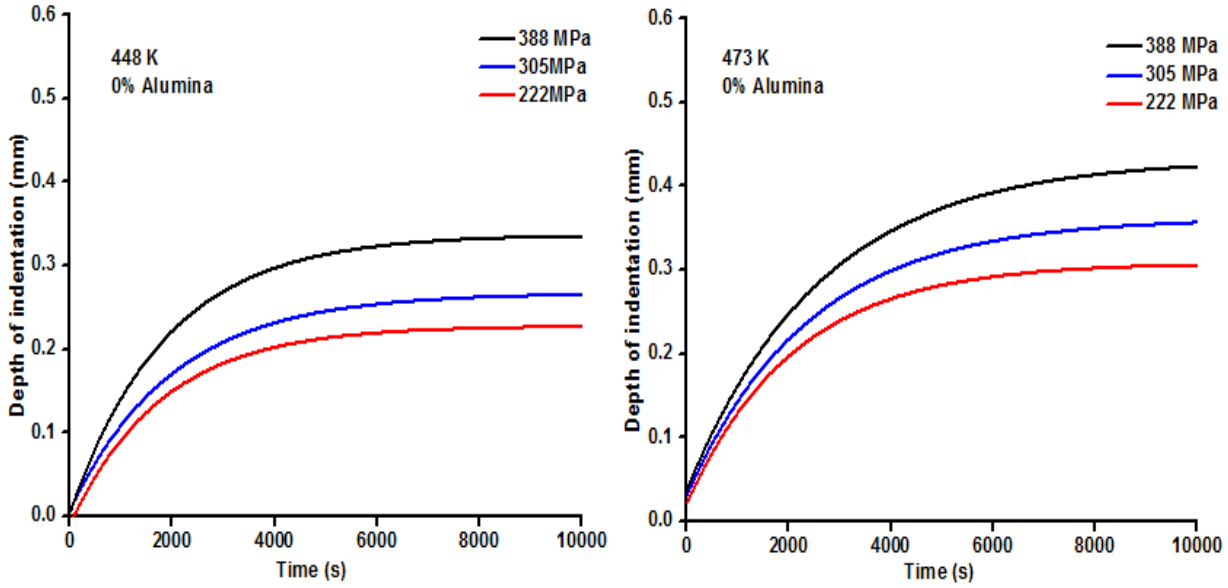

(a)

(b)

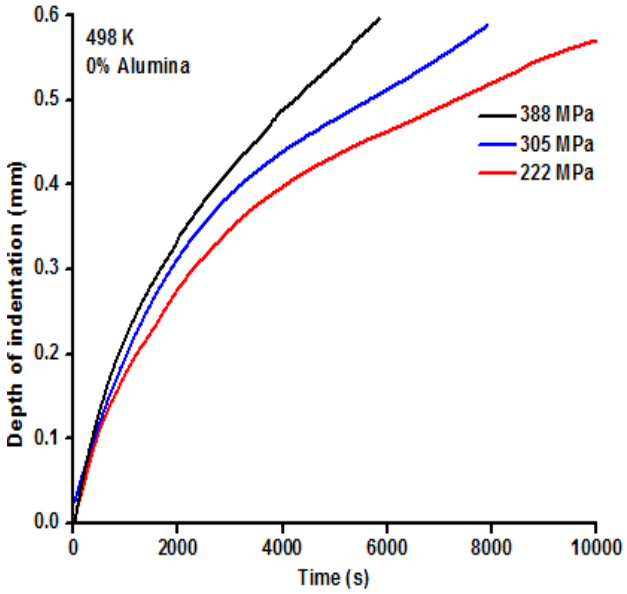

(c)

Fig. 6.7- Creep curves for as cast AZ91 tested at (a) 448 K, (b) 473 K and (c) 498 K

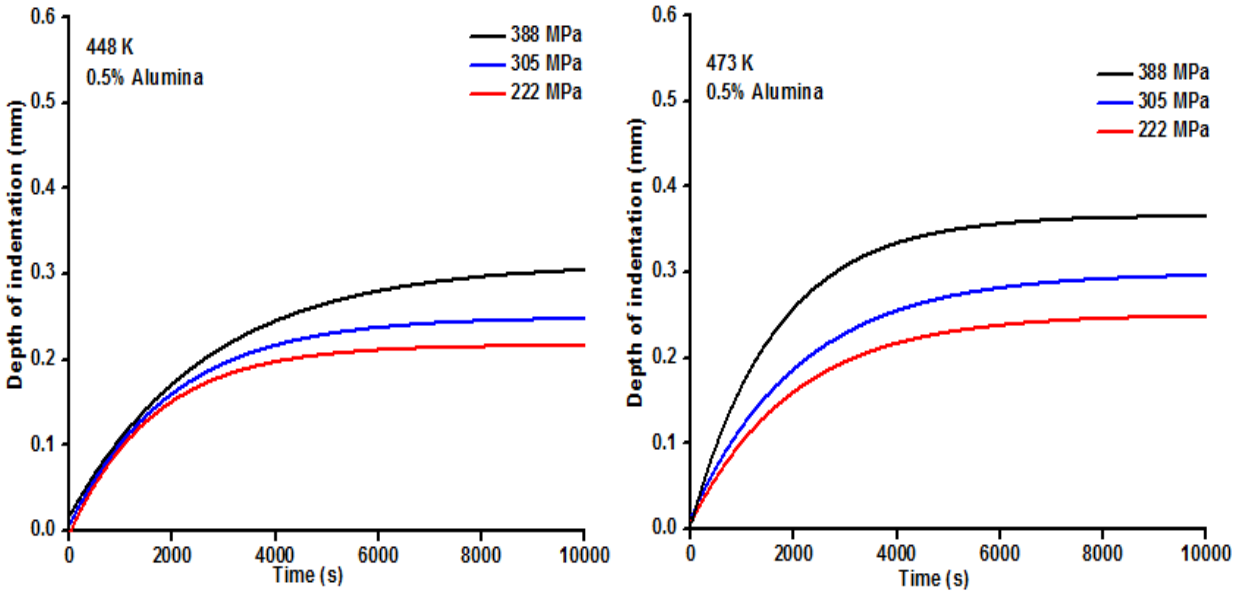

(a)

(b)

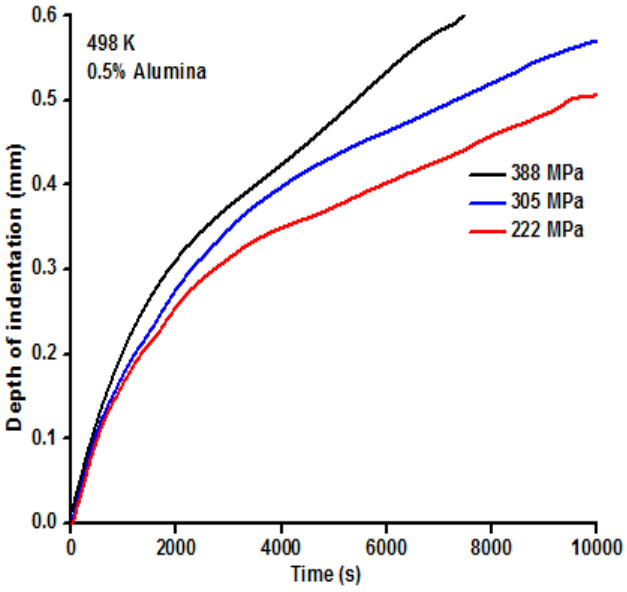

(c)

Fig.6.8- Creep curves for AZ91/0.5 wt% alumina composites tested at (a) 448 K, (b) 473 K and (c) 498 K

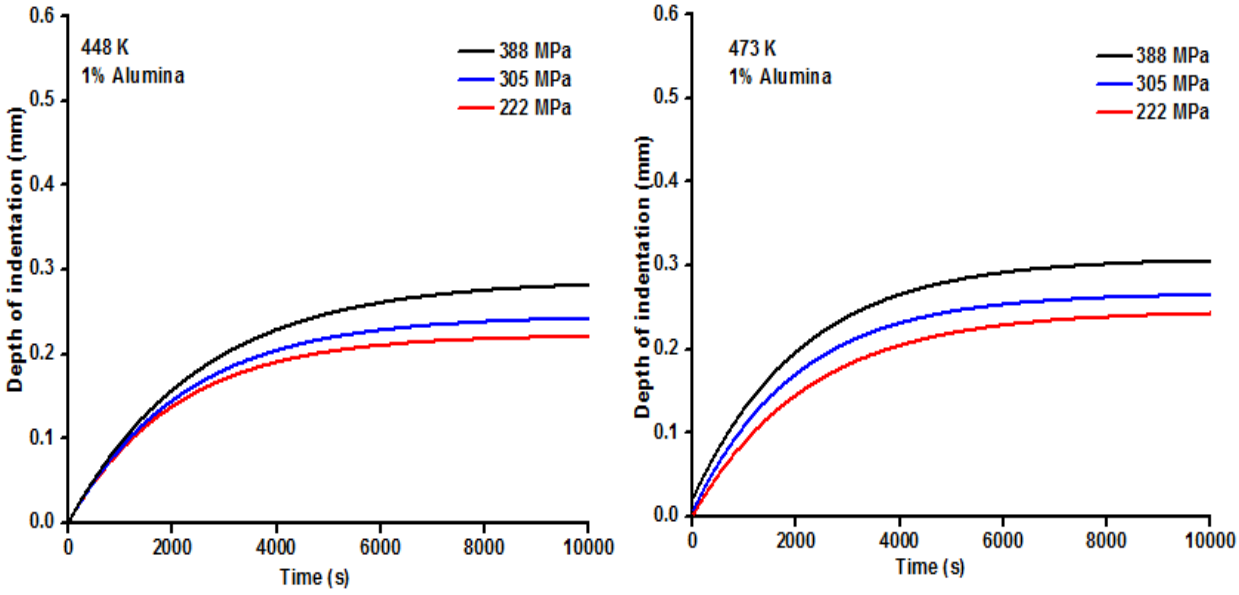

(a)

(b)

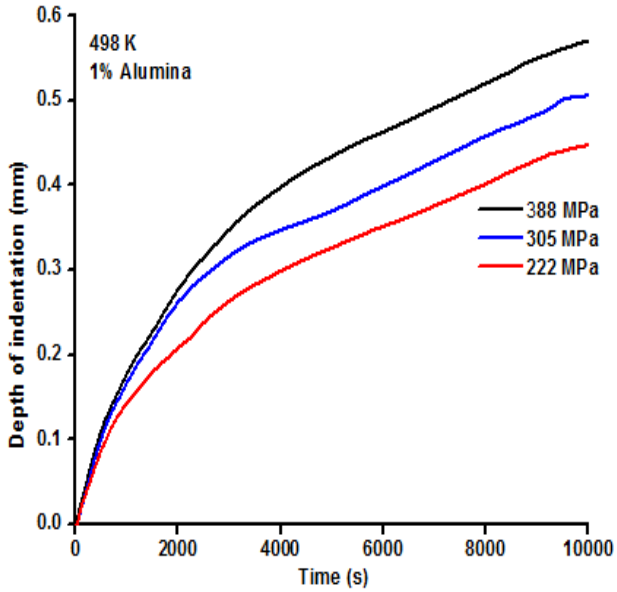

(c)

Fig.6.9- Creep curves for AZ91/1 wt% alumina composites tested at (a) 448 K, (b) 473 K and (c) 498 K

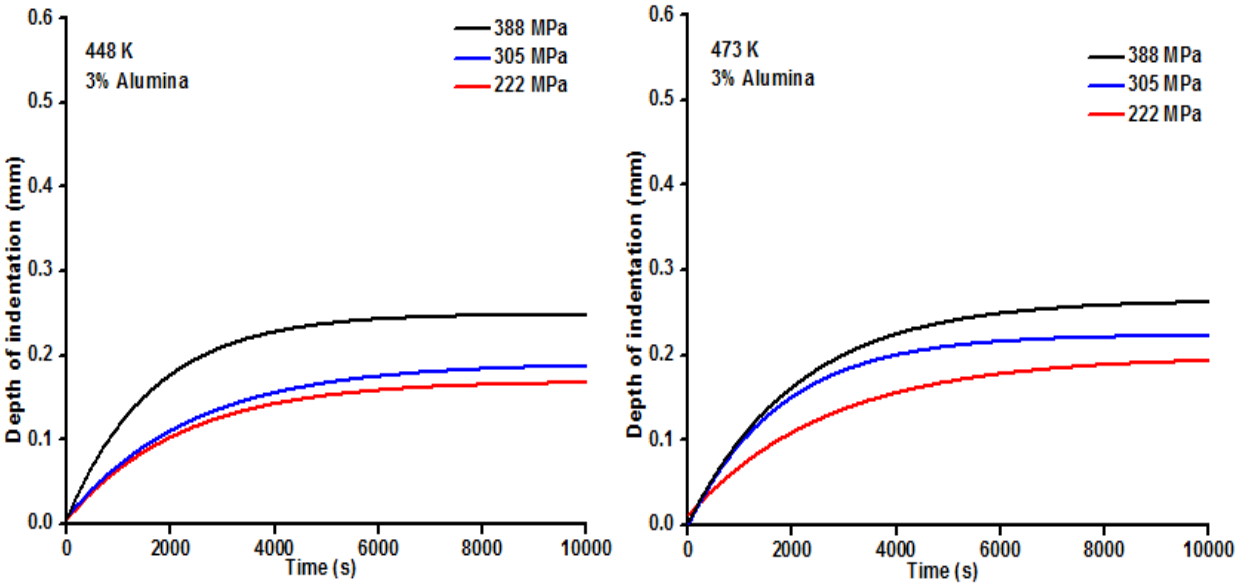

(a)

(b)

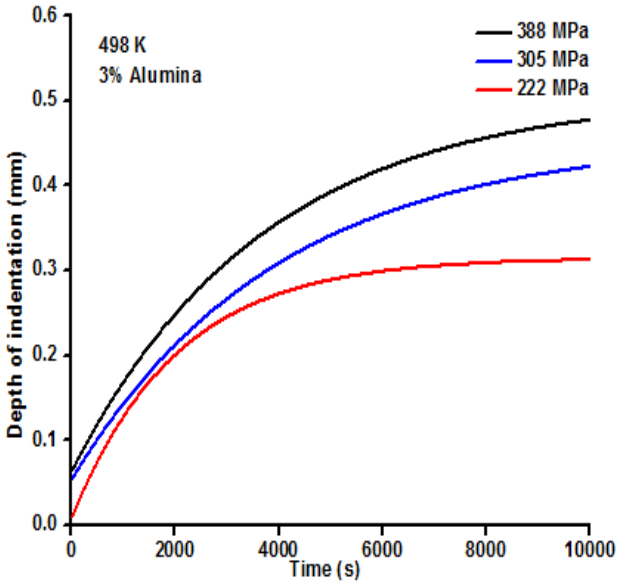

(c)

Fig.6.10- Creep curves for AZ91/3 wt% alumina composites tested at (a) 448 K, (b) 473 K and (c) 498 K

It can be seen in the creep curves, there is a decrease in creep rate with time during the primary stage as dislocation density increases due to which material gets work hardened. But balance between work hardening and recovery occurs during second stage or region. Hence creep rate is nearly constant in the secondary region. Also creep rate is increasing with stress and temperature as observed from all the creep graphs. Primary region is small at temperature of 448 K for the AZ91 nano composites. But at temperature of 498 K, accelerated creep is seen for them. Nano alumina additions increase the creep resistance of AZ91 alloy matrix with AZ91/3% alumina exhibiting the highest resistance. The same can be inferred from the plots. Minimum creep rate ε̇observed during the second stage is expressed by equation 6.1

$$\dot{\varepsilon} = \frac{\partial h}{\partial t} \tag{6.1}$$

Where 'h' and 't'denote depth of indentation in mm and time in seconds, respectively.

Equation 6.2 gives the mathematical expression for steady state creep

$$\dot{\varepsilon} = \frac{A\sigma^{n}}{d^{q}T}\exp\left(-\frac{Q}{RT}\right) \tag{6.2}$$

Where n and q are the stress exponent and grain size exponent, respectively.

The power law relation expressed in equation [13], is used to determine the dominant creep mechanism.

$$\dot{\varepsilon} = \frac{\mathrm{AGbD_v}}{\mathrm{kT}}(\sigma/\mathrm{G})^{\mathrm{n}} \tag{6.3}$$

Diffusion coefficientD_v is defined as

$$\mathrm{D_{v=}\ D_0}\exp\left(-\frac{\mathrm{Q}}{\mathrm{kT}}\right) \tag{6.4}$$

where Q denotes activation energy. By combining equations 6.3 and 6.4

$$\dot{\varepsilon} = \frac{AG\mathrm{bD_0}}{kT}(\sigma/\mathrm{G})^{\mathrm{n}}\exp\left(-\frac{Q}{kT}\right) \tag{6.5}$$

According to Norton, the stress equation is

$$\dot{\varepsilon} = A\sigma^{n}\exp^{(-\frac{Q}{RT})} \quad (6.6)$$

Or $$\ln \dot{\varepsilon} = \ln A + nln\sigma - Q/RT \quad (6.7)$$

A straight line is obtained by plotting ln ε̇ and ln σ at a given constant temperature. The stress exponent 'n' value is given by slope of this line. As shown in figure 6.11, stress exponent is different at different temperatures. Table 6.4 summarizes obtained stress exponent values. The average stress exponent 'n' for the as cast AZ91 alloy, AZ91/0.5 wt% alumina, AZ91/1 wt% alumina and AZ91/3 wt% alumina are approximately 3.28, 3.51, 4.34 and 5.27, respectively.

From these values it is clear that power law creep or dislocation creep is the dominating creep mechanism. Figure 6.12 shows the $\ln \dot{\varepsilon}$ and $\ln d$ plot at 448 K from where conclusion drawn is that operating creep mechanism does not depend upon grain size (q=0). Despite a marginal grain size reduction for nano composites, creep rate decreased. Hence creep rate was not affected by decrease in grain size. On the other hand nano-Al_2O_3 particles reinforced in the AZ91 alloy matrix increase the creep resistance.

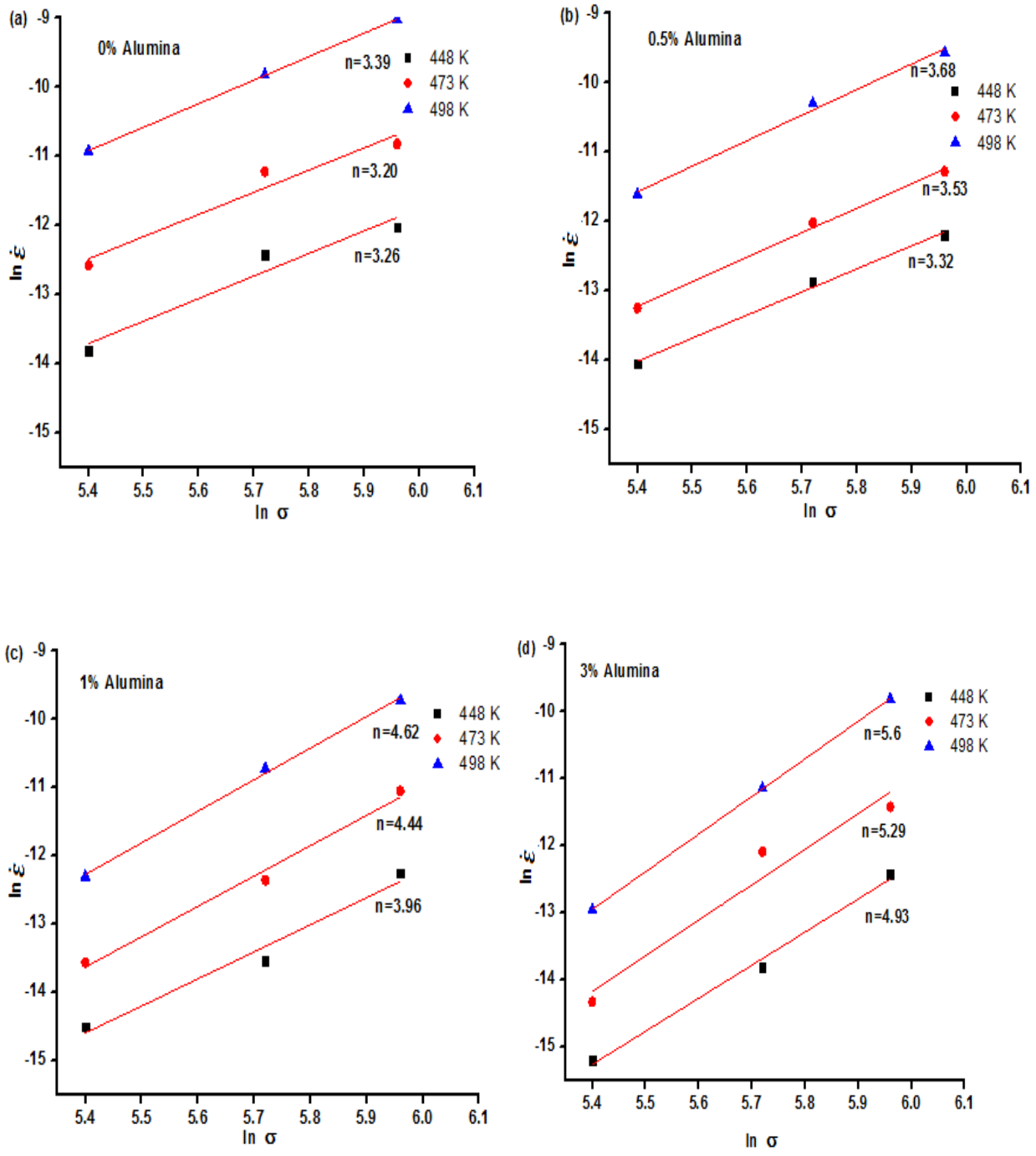

Fig.6.11-ln $\dot{\varepsilon}$ versus ln σ plot for (a) AZ91/0 wt% alumina, (b) AZ91/0.5 wt% alumina, (c) AZ91/1 wt% alumina, (d) AZ91/3 wt% alumina

Table 6.4 Stress exponent values for various processed nano composites

Composite	**Creep test temperature, K**	**Stress exponent 'n'**
AZ91-0 % Al_2O_3	448 K	3.26
	473 K	3.20
	498 K	3.39
AZ91-0.5% Al_2O_3	448 K	3.32
	473 K	3.53
	498 K	3.68
AZ91-1% Al_2O_3	448 K	3.96
	473 K	4.44
	498 K	4.62
AZ91-3% Al_2O_3	448 K	4.93
	473 K	5.29
	498 K	5.6

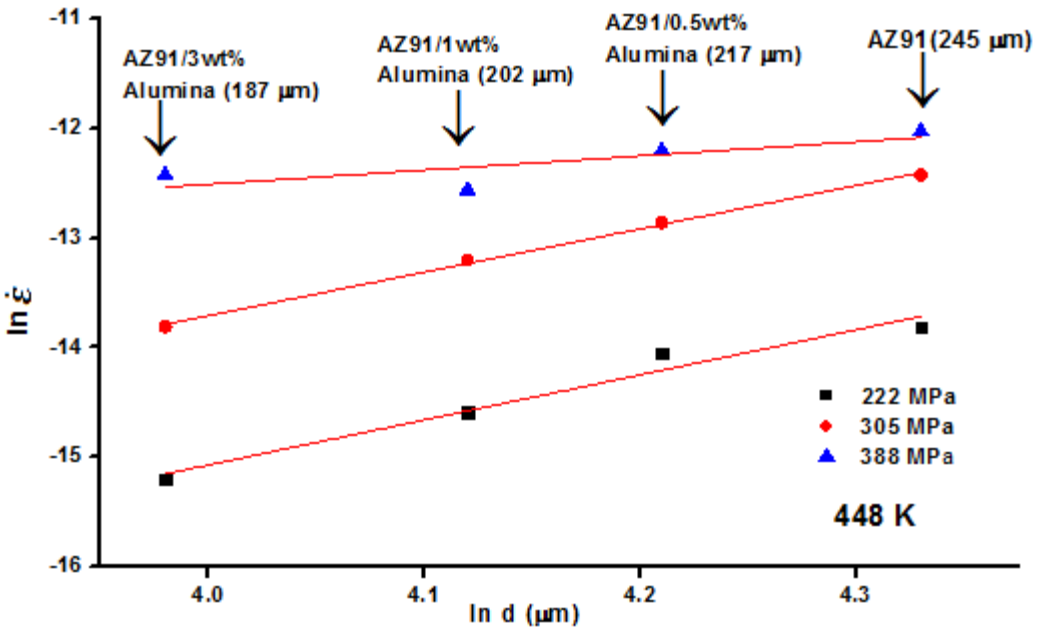

Fig.6.12- Plot of ln $\dot{\varepsilon}$ versus ln d at 448 K. The number in parenthesis is the average grain size of respective composite.

Equation 6.8 gives the expression given by Arrhenius for steady state creep rate

$$\dot{\varepsilon} = Ae^{-Q/RT} \qquad (6.8)$$

Figure 6.13 shows the plots between ln $\dot{\varepsilon}$ and 1/T for different stresses. From these plots straight line is obtained, slope of which is Q/R. R is the universal gas constant having value 8.314J/mol. Thus the value of activation energy Q can be calculated using these plots.

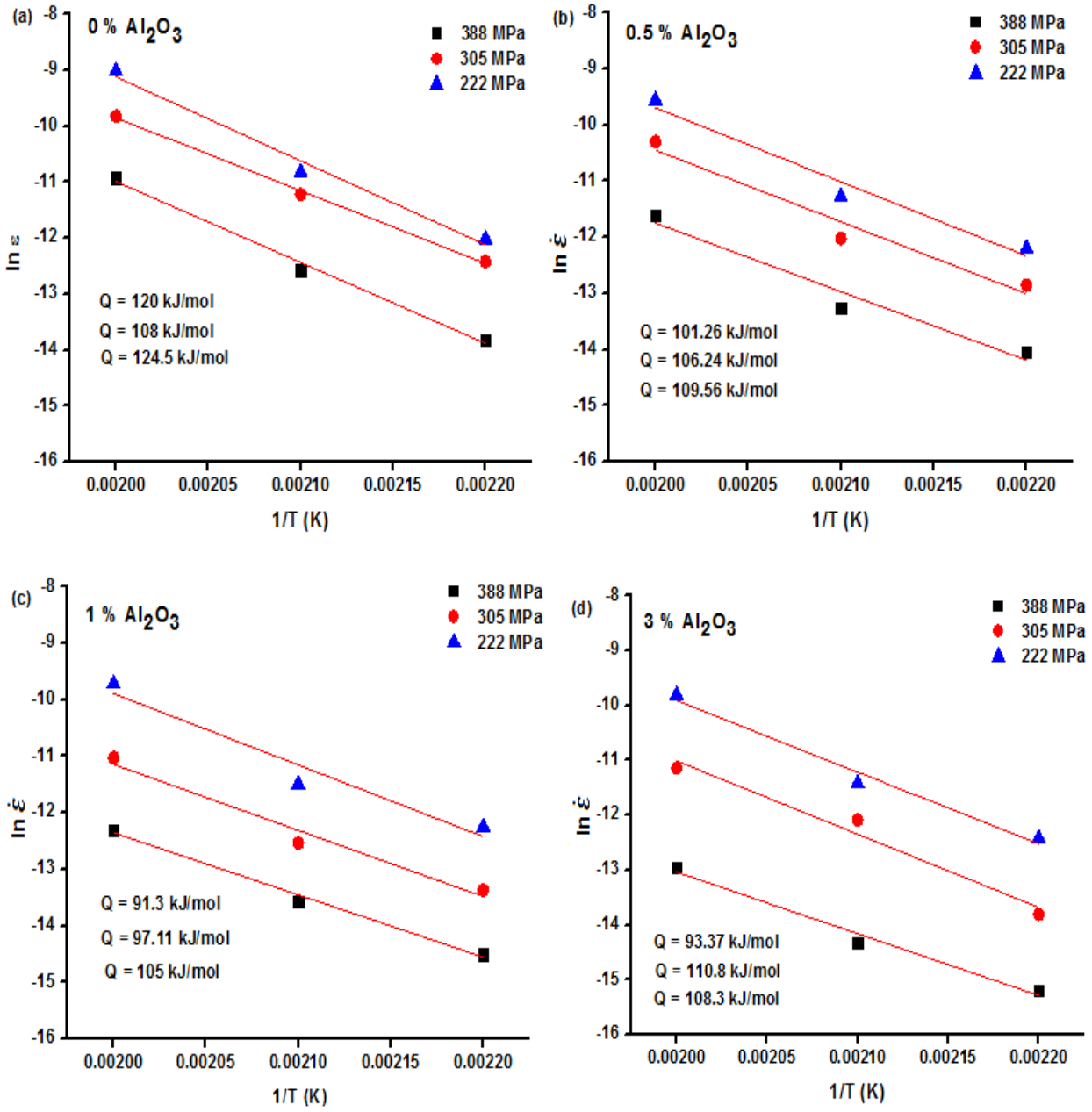

Fig. 6.13- Plot between ln $\dot{\varepsilon}$ and 1/T (K) for (a) AZ91/0 wt% alumina, (b) AZ91/0.5 wt% alumina, (c) AZ91/1 wt% alumina, (d) AZ91/3 wt% alumina at 222 MPa, 305 MPa and 388 MPa

For the as cast AZ91, AZ91/0.5% alumina, AZ91/1% alumina and AZ91/3% alumina composites, the calculated values of mean activation energies are 117.5kJ/mol, 105.68kJ/mol, 97.80kJ/mol and 104.15kJ/mol respectively. Inference can be drawn from these plots that at lower stress, values of activation energies are high and they decrease with increase in the

punching stress. Similar conclusions have been drawn by other researchers also [19, 20] where the activation energies showed a decreasing trend. At higher stress, activation energies values are close to that of dislocation pipe diffusion (92.5kJ/mol). Whereas at lower stress, they lie in between pipe diffusion and lattice diffusion (135kJ/mol) for magnesium. Thus, there is transition of creep controlling mechanism from dislocation pipe diffusion at high stress level to lattice diffusion at low stresses. Hence parallel to pipe diffusion, another mechanism that is lattice diffusion is activated. Each of the processes contributes to overall creep strain in case when parallel creep mechanisms are operating. But minimum creep rate is controlled by the faster among them.

Creep resistance of AZ91/nano alumina composites is improved mainly by addition of nano alumina particles. Uniform dispersion of these nano particles is achieved by high intensity ultrasound. Inter particle spacing between them decreases as we increase the weight fraction of nano alumina particles. From equation 2.2 as Orowan stress is inversely proportional to inter particle distance, it significantly influences creep rate. Utilizing parameters obtained in table 6.2 and taking shear modulus G = 16 GPa and burgers modulus b = 0.321 nm and keeping them in equation 2.2, the estimated increase in yield stress due to Orowan mechanism is shown in table 6.5.

Table 6.5- Estimated increase in yield stress due to Orowan mechanism

Mg alloy nano composite	Average size of nano particles (nm)	Inter-particle distance (nm)	τ_{Oro} (MPa)
AZ91/0.5 wt% Al_2O_3	77	359	10.2 MPa
AZ91/1 wt% Al_2O_3	98	278	13.74 MPa
AZ91/3 wt% Al_2O_3	122	124	31.98 MPa

At high temperature low melting secondary phase $Mg_{17}Al_{12}$ becomes soft and decreases strength of alloy matrix. Addition of nano alumina particles which are insoluble in matrix helps in retaining strength at higher temperature. Dislocations are difficult to cut through these hard nano particles, thus improving creep resistance of Mg alloy matrix.

7. CONCLUSIONS

Mechanical and Creep behavior of ultrasonically processed AZ91-nano alumina composite was studied. Different nano composites were cast by varying the weight percentage of nano alumina powder together with the use of mechanical stirring and ultrasonication. Microstructure characterization, mechanical and impression creep tests were carried out. The various conclusions drawn are listed.

1. Optical microscopy reveals the presence of low melting β-$Mg_{17}Al_{12}$ phase which deteriorates creep properties of AZ91. Less agglomeration and more uniform dispersion of nano alumina particles were observed during SEM analysis. XRD analysis confirms the additional alumina peaks.

2. Room temperature hardness and tensile properties got enhanced due to hard alumina particles blocking the movement of dislocations and thus providing strength.

3. There was improvement in the creep resistance property for the AZ91/nano-alumina composites with AZ91/3 wt% Al_2O_3 showing the best creep resistance among all. Orowan strengthening by nano alumina is responsible for this behavior.

4. The stress exponent values for various cast composites ranges from 3.28 to 5.27. It indicates dislocation creep as dominant creep mechanism.

5. At higher stress, dislocation pipe diffusion is controlling creep rate. Whereas at lower stress, parallel to pipe diffusion, another mechanism that is lattice diffusion is activated. Hence minimum creep rate is controlled by the faster among them.

8. SCOPE FOR FUTURE WORK

1. Transmission Electron Microscope (TEM) analysis can be carried out for the as cast and synthesized nano composites to closely study particle matrix interface.

2. SEM technique can be done to investigate the fracture behavior of AZ91/ nano alumina composites. In depth slip and dislocation analysis can be done for tensile and crept samples under Transmission Electron Microscopy (TEM).

9. REFERENCES

1. J. Lan, Y. Yang and X. Li: Microstructure and microhardness of SiC nanoparticles reinforced magnesium composites fabricated by ultrasonic method, Materials Science and Engineering: A, 2004, vol 386, pp. 284–290.

2. Y. Guangyin, S. Yangshan and D**.** Wenjiang: Effects of bismuth and antimony additions on the microstructure and mechanical properties of AZ91 magnesium alloy, Materials Science and Engineering: A, 2001, vol 308, pp 38-42.

3. K. Purazrang: Investigation of the mechanical behaviour of magnesium composites, Composites, 1994, vol 25, pp 296-302.

4. G. Cao: Study on tensile properties and microstructure of cast AZ91D/AlN nano composites, Materials Science and Engineering: A, 2008, vol 494, pp 127-131.

5. N. Srivastava, G.P. Chaudhari: Strengthening in Al alloy nano composites fabricated by ultrasound assisted solidification technique, Materials Science and Engineering: A, 2016, vol 651, pp 241-247.

6. S. Djordjevic: The Effects of Ultrasonic Solidification on aluminium, Journal of Mining and Metallurgy, 2003, vol 39, pp 527-532.

7. A.I.Y. Tok, F.Y.C. Boey, X.L Zhao: Novel synthesis of Al2O3 nano-particles by flame spray pyrolysis, Journal of Materials Processing Technology, 2006, 178 (2006) 270–273.

8. M. Paramsothy: The synergistic ability of Al_2O_3 nanoparticles to enhance mechanical response of hybrid alloy AZ31/AZ91, Journal of Alloys and Compounds, 2011, vol 509, pp 7572-7578.

9. A. Ramirez, Ma Qian, B.Davis, T. Wilks and D.H. St John: Potency of high -intensity ultrasonic treatment for grain refinement of magnesium alloys, Scripta Materialia, 2008, vol 59, pp 19-22.

10. S. Djordjevic: The Effects of Ultrasonic Solidification on aluminium, Journal of Mining and Metallurgy, 2003, vol 39, pp 527-532.

11. N.E. Dowling, Mechanical Behavior of Materials, Prentice-Hall, Upper Saddle River, New Jersey, 1999.

12. G.E. Dieter, Mechanical Metallurgy, SI Metric ed., McGraw-Hill (UK), 1988.

13. H.E. Friedrich, B.L. Mordike, Magnesium Technology, Berlin Heidelberg: Springer-Verlag, 2006.

14. H.J. Frost and M.F. Ashby, "Deformation-Mechanism maps", (Oxford, Pergamon Press), 1982.

15. A. Srinivasan, K.K. Ajithkumar, J. Swaminathan, U.T.S. Pillai': Creep Behavior of AZ91 Magnesium Alloy, Materials Science and Engineering: A, 2013, vol 55, pp 109-113.

16. H. Kumar, G.P. Chaudhari: Creep behavior of AS41 alloy matrix nano composites, Materials Science and Engineering: A, 2014, vol 607, pp 435-444.

17. Diao Yu-Shou, Lin Wie-Li,Qie Xi-Zhou (2015 January), Microstructure and high temperature creep property of nano Al_2O_3/6063Al composite synthesized by ultrasonic in-situ reaction, retrieved from fhclb.buaa.edu.cn/EN/volume/home.shtml.

18. S.F. Hassan, M. Gupta: Effect of particulate size of Al_2O_3 reinforcement on microstructure and mechanical behavior of solidification processed elemental Mg, Journal of Alloys and Compounds 2006, vol 419, pp 84-90.

19) R. Mahmudi, S. Moeendarbari: Effects of Sn additions on the microstructure and impression creep behavior of AZ91 magnesium alloy, Materials Science and Engineering: A, 2013, vol 566, pp 30-39.

20) F. Kabirian, R. Mahmudi: Effects of rare Earth Element Additions on the Impression Creep behavior of AZ91 magnesium alloy, Materials Science and Engineering: A, 2009, vol 20, pp 2190-2201.